



Sensor-free Soil Moisture Sensing Using LoRa Signals

ZHAOXIN CHANG, Institut Polytechnique de Paris, France and Institute of Software, Chinese Academy of Sciences, China

FUSANG ZHANG, Institute of Software, Chinese Academy of Sciences and University of Chinese Academy of Sciences, China

JIE XIONG, University of Massachusetts Amherst, United States

JUNQI MA, Beijing University of Posts and Telecommunications and Institute of Software, Chinese Academy of Sciences, China

BEIHONG JIN, Institute of Software, Chinese Academy of Sciences and University of Chinese Academy of Sciences, China

DAQING ZHANG, Institut Polytechnique de Paris, France and Peking University, China

Soil moisture sensing is one of the most important components in smart agriculture. It plays a critical role in increasing crop yields and reducing water waste. However, existing commercial soil moisture sensors are either expensive or inaccurate, limiting their real-world deployment. In this paper, we utilize wide-area LoRa signals to sense soil moisture without a need of dedicated soil moisture sensors. Different from traditional usage of LoRa in smart agriculture which is only for sensor data transmission, we leverage LoRa signal itself as a powerful sensing tool. The key insight is that the dielectric permittivity of soil which is closely related to soil moisture can be obtained from phase readings of LoRa signals. Therefore, antennas of a LoRa node can be placed in the soil to capture signal phase readings for soil moisture measurements. Though promising, it is non-trivial to extract accurate phase information due to unsynchronization of LoRa transmitter and receiver. In this work, we propose to include a low-cost switch to equip the LoRa node with two antennas to address the issue. We develop a delicate chirp ratio approach to cancel out the phase offset caused by transceiver unsynchronization to extract accurate phase information. The proposed system design has multiple unique advantages including high accuracy, robustness against motion interference and large sensing range for large-scale deployment in smart agriculture. Experiments with commodity LoRa nodes show that our system can accurately estimate soil moisture at an average error of 3.1%, achieving a performance comparable to high-end commodity soil moisture sensors. Field studies show that the proposed system can accurately sense soil moisture even when the LoRa gateway is 100 m away from the LoRa node, enabling wide-area soil moisture sensing for the first time.

CCS Concepts: • Human-centered computing → Ubiquitous and mobile computing systems and tools.

Additional Key Words and Phrases: Long range sensing; LoRa; Soil moisture sensing.

Authors' addresses: Zhaoxin Chang, Telecom SudParis, Institut Polytechnique de Paris, Evry, France; Institute of Software, Chinese Academy of Sciences, Beijing, China; Email: zhaoxin.chang@telecom-sudparis.eu. Fusang Zhang, State Key Laboratory of Computer Sciences, Institute of Software, Chinese Academy of Sciences; University of Chinese Academy of Sciences, Beijing, China; State Key Laboratory for Novel Software Technology, Nanjing University, Nanjing, China; E-mail: fusang@iscas.ac.cn. Jie Xiong, College of Information and Computer Sciences, University of Massachusetts Amherst, United States; E-mail: jxiong@cs.umass.edu. Junqi Ma, Beijing University of Posts and Telecommunications; Institute of Software, Chinese Academy of Sciences, Beijing, China; E-mail: junqi_ma@bupt.edu.cn. Beihong Jin, State Key Laboratory of Computer Sciences, Institute of Software, Chinese Academy of Sciences; University of Chinese Academy of Sciences, Beijing, China; E-mail: Beihong@iscas.ac.cn. Daqing Zhang, Telecom SudParis, Institut Polytechnique de Paris, Evry, France; School of Computer Science, Peking University, Beijing, China, E-mail: dqzhang@sei.pku.edu.cn. Corresponding Author: Daqing Zhang, Fusang Zhang; E-mail: dqzhang@sei.pku.edu.cn, fusang@iscas.ac.cn.

Permission to make digital or hard copies of all or part of this work for personal or classroom use is granted without fee provided that copies are not made or distributed for profit or commercial advantage and that copies bear this notice and the full citation on the first page. Copyrights for components of this work owned by others than ACM must be honored. Abstracting with credit is permitted. To copy otherwise, or republish, to post on servers or to redistribute to lists, requires prior specific permission and/or a fee. Request permissions from permissions@acm.org.

© 2022 Association for Computing Machinery.

2474-9567/2022/6-ART45 \$15.00

<https://doi.org/10.1145/3534608>

ACM Reference Format:

Zhaoxin Chang, Fusang Zhang, Jie Xiong, Junqi Ma, Beihong Jin, and Daqing Zhang. 2022. Sensor-free Soil Moisture Sensing Using LoRa Signals. *Proc. ACM Interact. Mob. Wearable Ubiquitous Technol.* 6, 2, Article 45 (June 2022), 27 pages. <https://doi.org/10.1145/3534608>

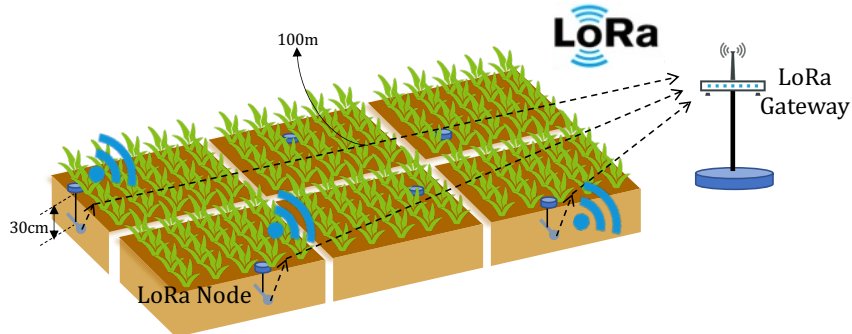


Fig. 1. Sensing soil moisture using LoRa signals.

1 INTRODUCTION

Fresh water is one of the most precious natural resources on earth. 70% of the world's fresh water is used for irrigation and approximately 60% of that is actually wasted [1][11]. In recent years, precision irrigation attracted a lot of attention as it plays a key role in saving water and increasing crop yields. By optimizing irrigation using soil moisture monitoring, 80% of the water currently wasted in irrigation can be saved [64]. To enable precision irrigation, the most important information needs to be acquired is soil moisture. Existing soil moisture sensing systems are mainly based on dedicated sensors. High-end soil moisture sensors can achieve a high accuracy. These sensors rely on highly accurate time-of-flight measurements to obtain the speed of signal propagation in the soil [60, 63]. The signal propagation speed is then utilized to infer the soil moisture. To achieve highly accurate time measurement, expensive oscillator is required which leads to high cost of the moisture sensor (\$100-\$400) [8]. On the other hand, low cost soil moisture sensors (\$10-\$20) can achieve a coarse sensing accuracy with errors in the range of 5% to 15%, which cannot satisfy the requirement of many real-life applications, i.e., an error lower than 5% [44]. In the past few years, researchers utilized Radio Frequency (RF) signals such as WiFi [30] for low-cost soil moisture sensing. However, due to the short communication range and high power consumption, WiFi infrastructure is mostly limited to indoor environments and is not available in smart agriculture scenarios. Different from WiFi, low-power wide-area LoRa technology is designed for long-range communication which is ideal for outdoor agricultural scenarios. In recent years, LoRa infrastructure has been actively deployed on farmlands. It is expected that 2.5 million LoRa nodes will be deployed by the end of 2024 [3]. However, for current LoRa infrastructure, only the data communication function is utilized.

In this work, we propose to leverage LoRa signal itself as a sensing tool to measure soil moisture without a need of any dedicated sensors. The basic principle behind this is that the dielectric permittivity of soil varies with soil moisture and the dielectric permittivity determines the propagation speed of LoRa signal in the soil. As the signal frequency does not change, the signal wavelength changes with signal speed. As one wavelength of signal propagation induces a phase change of 2π , different phase readings can be measured with different soil moisture values. By measuring the phase change caused by a fixed amount of signal propagation distance in the soil, the soil dielectric permittivity can be obtained, and accordingly soil moisture can be estimated. Figure 1 shows the

envisioned application scenario of the proposed method. The antennas of LoRa nodes are plugged in the soil. The LoRa nodes serve as the transmitter while the LoRa gateway serves as the receiver which can be connected to tens of LoRa nodes. By just sending one LoRa packet from the LoRa node to gateway, soil moisture can be accurately estimated. Though the main idea sounds straightforward, to turn the idea into a working system, multiple challenges need to be tackled.

Due to the narrow bandwidth (i.e., 125 kHz - 500 kHz) of LoRa signals, the signal propagation time can not be accurately obtained for speed estimation owing to the low sampling rate. For example, a sampling rate of 1 MHz can only present sample-level ($1 \mu s$) granularity in time measurement which is far from enough to measure the subtle time change, i.e., a few nanoseconds, caused by soil moisture change. Recent works propose to use fine-grained signal phase change to measure sub-sample level signal propagation time [74]. In this work, we adopt the phase-based method to obtain fine-grained time information for speed estimation. However, one challenge is encountered when we apply the phase-based method to our system. Specifically, to achieve accurate phase measurement, we would like the amount of phase change caused by soil moisture to be large. However, we observe that soil moisture has a big impact on phase changes, i.e., the phase change can be six times larger when soil moisture is high compared to that when soil moisture is low. In soil moisture sensing, the signal propagation length in the soil depends on how deep the antenna is plugged in the soil. Even we assume the propagation distance in soil is just 20 cm, the signal phase change in soil can still easily exceed 2π . For example, when the soil moisture is 40%, the propagation speed of signal in the soil is one-fifth that in the air (i.e., $c' = \frac{1}{5}c_0$, $c_0 = 3 \times 10^8 m/s$). Thus, the phase change for a propagation distance of 20 cm in the soil is $2\pi f_c \frac{20cm}{c'} = 6.1\pi$, where $f_c = 915MHz$ is the carrier frequency of LoRa signal. In this case, the phase change will be wrapped within the range of 0 and 2π , causing the issue of phase ambiguity. Therefore, *how to address the phase ambiguity issue caused by a phase change larger than 2π is the first challenge when we apply phase readings for soil moisture sensing.*

To tackle this challenge, we propose a dual-antenna design at the LoRa node side. Instead of measuring the phase change caused by the entire signal propagation path in the soil, we calculate the phase difference between the two antennas, making the phase measurement independent of the soil depth. We further carefully design the antenna spacing to ensure the amount of phase change will never exceed 2π and at the same time make sure the two antennas are not placed too close which can cause antenna coupling.

To enable dual-antenna design, we include a cheap RF switch (\$3.75) to support LoRa node which has just one RF front end to be connected to two antennas. With the help of the RF switch, the LoRa node can transmit signals from two antennas sequentially. However, we quickly realize obtaining accurate phase readings is non-trivial. As the LoRa node and gateway are not synchronized, there exists a time-varying phase offset at each packet received at the receiver, rendering the phase readings unusable. Existing methods [72][74] employ two antennas at the receiver which share the same clock to cancel out the phase offset. However, this method can not be applied here because it also cancels out the phase change induced by the soil which is the information we need to extract for soil moisture sensing. Therefore, *the second challenge is how to remove the random signal phase offset without corrupting the phase information critical for soil moisture sensing.*

We propose to employ the two antennas at the transmitter side to address the issue of phase offset. This is very different from existing methods which have two antennas at the receiver side [72][74]. The key difference is that while receiver side methods capture one single transmission at two receiver antennas, the proposed transmitter side method sends out two transmissions sequentially from two transmitter antennas. Two sequentially transmitted signals can have different phase offsets and therefore the phase offsets may not be canceled out. To deal with this issue, we propose delicate signal processing to cancel the phase offset at chirp level (milliseconds) rather than at packet level (seconds). We make the antenna switching happen within one LoRa packet instead of between packets. Within a short period of time, we show the carrier frequency offset (CFO) can be safely assumed as a constant. We therefore propose a chirp ratio approach, which performs a division operation on two

adjacent chirps. In order to obtain the ratio of two chirps, the two chirps need to be accurately segmented. We find this a challenging task in practice because there exists sampling time offset between adjacent chirps. We propose to upsample the raw LoRa signal to mitigate the effect of sampling time offset and segment the chirps accurately for the ratio operation.

To demonstrate the effectiveness of the proposed approaches, we implement the proposed soil moisture sensing system based on commodity LoRa node and USRP-based LoRa gateway. Comprehensive experiments are conducted to evaluate the system performance under different conditions. The results show that our system can monitor soil moisture at an average error of 3.1%, comparable to that obtained from high-end soil moisture sensors. Our system can still achieve reasonably high accuracy when the distance between LoRa node and gateway is 100 m. The main contributions of this work are summarized as below:

- To the best of our knowledge, this is the first work to enable long-range and high-accuracy soil moisture sensing using LoRa signals, enabling wide-area soil moisture sensing for the first time.
- We propose a dual-antenna design with carefully planned antenna spacing to address the issue of phase ambiguity. We further propose a chirp ratio approach to eliminate the effect of random phase offset. The proposed design just requires one packet transmission to accomplish soil moisture sensing.
- We prototype our design and showcase the effectiveness of the proposed system with both laboratory and field experiments. Comprehensive experiments demonstrate its superior performance in terms of accuracy (comparable to high-end moisture sensor), sensing range (up to 100 m), deployment flexibility and robustness against interference.

2 PRELIMINARIES

2.1 Radio Frequency Based Soil Moisture Sensing

The principle of RF-based soil moisture sensing is that the dielectric permittivity of soil varies with soil moisture. The permittivity change causes the propagation speed of RF signal in soil to change and we can therefore infer the soil moisture by measuring the signal propagation speed in the soil. The dielectric permittivity is a physical property of a material and is determined by the polarity of the molecules that make up the material. The stronger the polarity of the molecules in the material, the larger the dielectric permittivity, and accordingly the slower the propagation speed in this material [36]. The propagation speed of RF signal in a particular material (e.g., water or soil) can be expressed as:

$$c = \frac{c_0}{\sqrt{\epsilon}}, \quad (1)$$

where $c_0 = 3 \times 10^8 \text{ m/s}$ is the speed of RF signal in free space and ϵ is the dielectric permittivity of the material, which determines the speed of signal propagation in this material. Thus, by measuring the speed of RF signal in the material, ϵ can be estimated. The propagation speed of RF signal in the air and that in free space are approximately equal, i.e., $\epsilon_{\text{air}} = 1$. For water, $\epsilon_{\text{water}} = 80.1$ which indicates a much smaller speed. For soil, as the moisture increases, the water content in the soil gradually increases, causing ϵ_{soil} to gradually rise. The dielectric permittivity of soil is typically between 3 and 40 [42]. It has been proved that there is an empirical relationship between the soil moisture and the dielectric permittivity [63]:

$$\Theta = 4.3 \times 10^{-6} \epsilon_{\text{soil}}^3 - 5.5 \times 10^{-4} \epsilon_{\text{soil}}^2 + 2.92 \times 10^{-2} \epsilon_{\text{soil}} - 5.3 \times 10^{-2}, \quad (2)$$

where Θ is the volumetric water content (VWC) in soil (i.e., numerical measure of soil moisture), defined as the ratio of the volume of water to the total volume of water and soil. In general, for soil moisture, the range of Θ is between 0% and 50%¹ [10, 25, 41]. Note that when the moisture is between 50% and 100%, the water and soil

¹In some literature [17], the absolute moisture range of 0 - 50% is scaled to 0 - 100%, which is a relative range corresponding to the absolute soil moisture range of 0 - 50% in this work.

actually become two separate layers. The “soil moisture” of pure water is 100%. For major agricultural crops such as wheat, corn and potato, the adequate soil moisture is between 10% to 35% [9, 31, 65].

2.2 LoRa Signals for Sensing

LoRa employs Chirp Spread Spectrum (CSS) modulation to achieve long-range communication. The basic LoRa transmission unit is a chirp, which is characterized by the carrier frequency f_c , chirp duration T , frequency bandwidth B and chirp slope $k = \frac{B}{T}$. Figure 2 shows the signal spectrum of a typical LoRa packet, which consists of three parts: preamble, start frame delimiter (SFD) and payload. Preamble is the start of a packet and contains several full up-chirps. SFD indicates the start of payload which is composed of down-chirps. In the payload part, data are encoded by varying the start frequency of each chirp.

To fully understand LoRa sensing, we first introduce the signal propagation model in the air. LoRa node generates a chirp signal and modulates it to the carrier frequency band (e.g., 915 MHz). Then the transmitted signal can be represented as follow:

$$S_T(t) = c(t)e^{j(2\pi f_c t + \phi_c)} = e^{j\pi(kt^2 - Bt)}e^{j(2\pi f_c t + \phi_c)}, \quad (3)$$

where $c(t) = e^{j\pi(kt^2 - Bt)}$ is the CSS modulated baseband chirp signal [70] and ϕ_c is the initial carrier signal phase at the transmitter. Then, the signal arriving at the receiver can be represented as:

$$S_R(t) = A_R S_T(t - \tau) = A_R c(t - \tau) e^{j(2\pi f_c(t - \tau) + \phi_c)}, \quad (4)$$

where A_R denotes the signal amplitude attenuation, $\tau = \frac{d}{c_0}$ is the time delay of signal propagation and d is the distance between LoRa transmitter and receiver. The LoRa receiver demodulates the received signal by multiplying it with $e^{-j(2\pi f'_c t + \phi'_c)}$, where f'_c is the carrier frequency at the receiver (gateway) and ϕ'_c is the initial phase of the gateway oscillator. Note that ideally the carrier frequency at the transmitter should be the same as the carrier frequency at the receiver, i.e., $f_c = f'_c$. In reality, there is always a small difference between f'_c and f_c which is called carrier frequency offset (CFO). The demodulated signal can then be represented as:

$$R(t) = A_R c(t - \tau) e^{j\Phi_{offset}} e^{j\Phi}, \quad (5)$$

where $\Phi_{offset} = 2\pi(f_c - f'_c)t + (\phi_c - \phi'_c)$ is the CFO-induced phase offset, and $\Phi = -2\pi f_c \tau$ is the phase change due to signal propagation path.

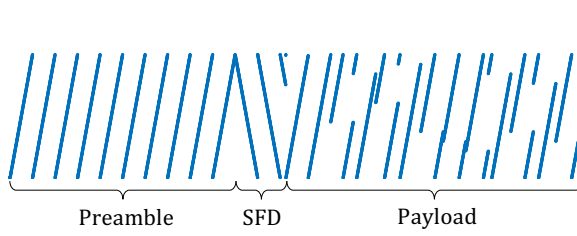


Fig. 2. An example of LoRa packet.

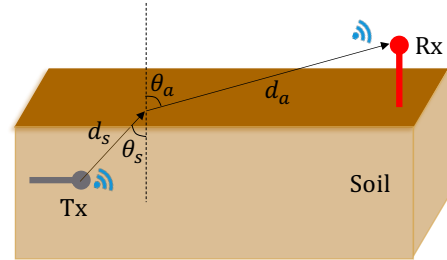


Fig. 3. Propagation model of LoRa signal.

2.3 Feasibility of Sensing Soil Moisture Using LoRa Signals

Before proposing our design, we first analyze the feasibility of using LoRa signal to sense soil moisture. First, we model the signal propagation from the LoRa node in soil to the gateway in air. As shown in Figure 3, the antenna of LoRa node is buried in soil and the gateway is placed above the ground in the air. LoRa signal is transmitted from the node and reaches the gateway through the refraction of the soil surface. d_s and d_a denote the path length

of signal in soil and air, respectively. θ_s and θ_a respectively represent the angle between the signal propagation path and the soil surface in soil and air. According to Equation 1, the speed of RF signal in soil is very different from that in air. The total time delay of signal can be expressed as:

$$\tau_{s2a} = \frac{d_s}{c} + \frac{d_a}{c_0} = \frac{\sqrt{\epsilon_s} d_s + d_a}{c_0}. \quad (6)$$

Thus, the signal at LoRa gateway can be written as:

$$R_{s2a}(t) = A_R c(t - \tau_{s2a}) e^{j\Phi_{offset}} e^{j\Phi_{s2a}}, \quad (7)$$

where $\Phi_{s2a} = -2\pi f_c \tau_{s2a}$ is the phase change due to signal propagation in the soil and in the air. It can be observed that Φ_{s2a} is related to the dielectric permittivity of the soil. However, Φ_{s2a} is sensitive to soil moisture and can easily exceed 2π . For example, the dielectric permittivity of the soil is $\epsilon_s = 25$ when the soil moisture is 40% according to Equation 2. Assume that $d_s = 20 \text{ cm}$, the phase change caused by the signal propagation in soil is calculated as $2\pi f_c \frac{\sqrt{\epsilon_s} d_s}{c_0} = 6.1\pi$, which exceeds 2π and will be wrapped to the range within 0 and 2π . In real world deployment, d_s might be even larger. Therefore, even Φ_{s2a} can be accurately extracted and the path length of the signal propagation (i.e., d_s and d_a) can be estimated, ϵ_s still can not be accurately estimated for soil moisture sensing due to the issue of phase ambiguity.

On the other hand, the phase of baseband chirp signal $c(t - \tau_{s2a})$ and the CFO-induced phase offset Φ_{offset} change rapidly over time. Therefore, the phase change caused by signal propagation path Φ_{s2a} can not be extracted from the original signal. In conclusion, the original LoRa signal can not be used to sense soil moisture directly due to the phase ambiguity issue and the effect of random phase offset.

3 SENSING SOIL MOISTURE USING LORA SIGNALS

In this section, we propose the detailed design of the proposed system. Figure 4 shows the overview of our proposed sensing system.

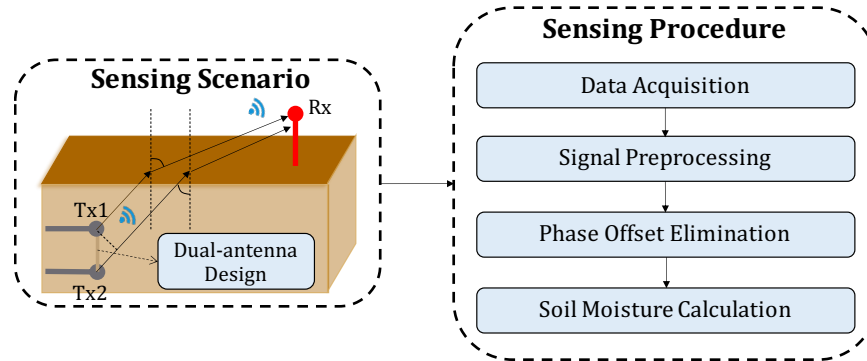


Fig. 4. Soil moisture sensing approach overview.

3.1 Dual-antenna Design for Soil Moisture Sensing

From the previous section, we know that the phase readings of LoRa signal are sensitive to soil moisture change and the change can exceed 2π easily. In this subsection, we explain when there are two antennas at the transmitter side, how can we leverage these two antennas to constrain the phase change to be below 2π for soil moisture sensing.

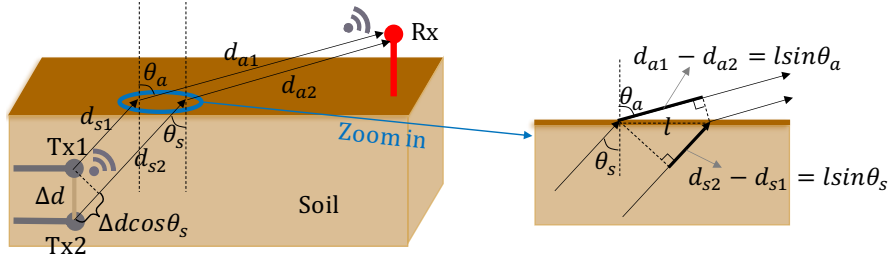


Fig. 5. Dual-antenna signal propagation model.

As shown in Figure 5, two transmitter antennas are denoted by Tx1 and Tx2, and the spacing between them is denoted as Δd . According to Equation 6, the phase change of signal propagation from Tx1 to Rx is $\Phi_{link1} = -2\pi f_c \frac{\sqrt{\epsilon_s} d_{s1} + d_{a1}}{c_0}$. The phase change of signal propagation from Tx2 to Rx can then be expressed as $\Phi_{link2} = -2\pi f_c \frac{\sqrt{\epsilon_s} (d_{s2} + \Delta d \cos \theta_s) + d_{a2}}{c_0}$. d_{s1} , d_{s2} , d_{a1} and d_{a2} denote the path length of two signal propagation links in soil and air, respectively. Note that according to the law of refraction, the incident angle θ_s and refraction angle θ_a of the signal satisfy the following equation $\sqrt{\epsilon_s} \sin \theta_s = \sin \theta_a$. Thus, $d_{a1} - d_{a2} = \sqrt{\epsilon_s} (d_{s2} - d_{s1})$. Therefore, the phase difference between these two propagation links is:

$$\Delta \Phi = \Phi_{link2} - \Phi_{link1} = -2\pi f_c \frac{(d_{a2} - d_{a1}) - \sqrt{\epsilon_s} (d_{s1} - d_{s2}) + \sqrt{\epsilon_s} \Delta d \cos \theta_s}{c_0} = -2\pi f_c \frac{\sqrt{\epsilon_s} \Delta d \cos \theta_s}{c_0}. \quad (8)$$

Based on Equation 8, the dielectric permittivity of soil can be calculated as: $\epsilon_s = \left(\frac{c_0 \Delta \Phi}{2\pi f_c \Delta d \cos \theta_s} \right)^2$. However, at LoRa receiver, we can only obtain the phase difference $\Delta \Phi$. This is not enough as we still need to know the value of θ_s to calculate ϵ_s . Fortunately, we prove that even without knowing the value of θ_s , ϵ_s can still be accurately estimated. We explain the reason below. We first assume $\theta_s = 0$ and the estimated dielectric permittivity of soil is:

$$\hat{\epsilon}_s = \left(\frac{c_0 \Delta \Phi}{2\pi f_c \Delta d} \right)^2, \quad (9)$$

with $\hat{\epsilon}_s = \epsilon_s (\cos \theta_s)^2$. Then, based on Equation 2, a soil moisture value $\hat{\Theta}$ can be calculated based on $\hat{\epsilon}_s$. When there is a non-zero angle between LoRa node and gateway, i.e., $\theta_s \neq 0$, $\cos \theta_s < 1$.

During the process of signal propagation from Tx to Rx, the signal is refracted at the soil surface. According to the law of refraction, $\sqrt{\epsilon_s} \sin \theta_s = \sin \theta_a$. Since ϵ_s is always greater than 1 (i.e., 3-40), θ_s is smaller than θ_a . The maximum value of θ_a is equal to 90° , and in this case, the incident angle can be calculated as:

$$\theta_{smax} = \arcsin \frac{1}{\sqrt{\epsilon_s}}. \quad (10)$$

Although there exists signals with an incident angle greater than θ_{smax} in the soil, these signals will not be refracted from the soil surface into the air, but will be totally reflected back into the soil as shown in Figure 6. This phenomena is called Total Internal Reflection (TIR) and θ_{smax} is called critical angle. The greater the dielectric permittivity, the smaller the critical angle. For soil, since ϵ_s is between 3 and 40, the corresponding critical angle θ_{smax} is between 30° and 9.6° .

To see the maximum error of soil moisture estimation caused by taking $\theta_s = 0^\circ$, we assume that the incident angle of the signal in the soil is equal to the critical angle, i.e., $\theta_s = \theta_{smax}$ at various soil moisture levels. Then, we calculate the estimated value of the dielectric permittivity $\hat{\epsilon}_s$ according to $\hat{\epsilon}_s = \epsilon_s (\cos \theta_s)^2$. We then put the true value and estimated value (assuming $\theta_s = 0$) of the dielectric permittivity into the Equation 2 to calculate the estimated value and the true value of soil moisture. Figure 7 shows the maximum potential error of soil moisture

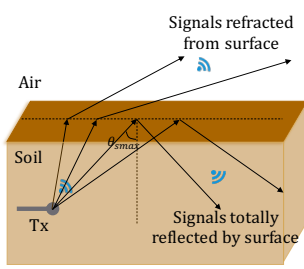


Fig. 6. An illustration of total internal reflection.

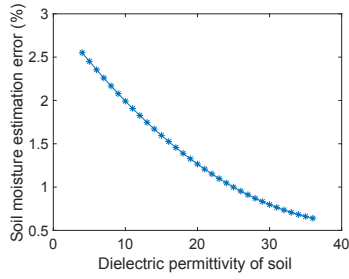


Fig. 7. The maximum soil moisture estimation error at different ϵ_s .

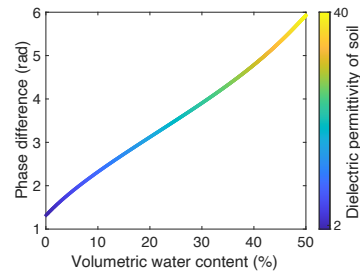


Fig. 8. The relationship between soil moisture and phase difference.

estimation is 2.6% when $\epsilon_s = 4$, and as the value of ϵ_s increases, the estimation error further decreases. Therefore, the maximum error of soil moisture estimation caused by the existence of θ_s is less than 2.6%, which means that in practice we can just assume $\theta_s = 0$ without a need to know the angle.

The dielectric permittivity of soil is generally between 3 and 40, thus, by carefully setting the antenna spacing Δd , we can make sure the phase difference is always lower than 2π , avoiding the issue of phase ambiguity. The conclusion is that if there is a dual-antenna configuration at the LoRa node, the phase difference of signals sent by the two antennas can be used to constrain the phase difference to be smaller than 2π and estimate the soil moisture. Figure 8 shows the relationship between soil moisture and phase difference when the antenna spacing Δd is 5 cm. It can be observed that when soil moisture varies between 0 - 50%, the maximum phase change does not exceed 2π . Unfortunately, commodity LoRa node is usually only equipped with one RF front end due to the low cost. How to equip the existing LoRa node with two antennas without significantly increasing the cost is a challenge. A straightforward solution is to use two LoRa nodes. However, this will double the cost of the system and also bring synchronization issue between LoRa nodes. Another simple solution is to connect a two-port power splitter to the RF front end of the LoRa node and connect one antenna to each port. In this way, the signal generated by the LoRa node can be sent from both antennas at the same time. However, signals transmitted from two antennas at the same time will interfere at the LoRa receiver, corrupting the phase reading of each individual propagation link.

In this work, we adopt a low-cost single-port-dual-throw (SPDT) RF switch [16] to enable the proposed dual-antenna design. The switch allows the signal to be sent from two antennas sequentially. To leverage such a dual-antenna design with the help of a switch to measure soil moisture, in the next few sections, we first reveal the effect of carrier frequency offset (CFO) on LoRa signals (Section 3.2). Then, we study the unique characteristic of CFO in LoRa and propose the antenna switching design for LoRa node (Section 3.3). Finally, we propose a delicate chirp ratio approach to cancel out the effect of CFO to enable fine-grained soil moisture sensing (Section 3.4).

3.2 The Effect of Carrier Frequency Offset (CFO)

In this subsection, we first introduce the effect of CFO on LoRa signals transmitted from different antennas. CFO is caused by the unsynchronized clocks of LoRa transceivers. When LoRa transceivers start working, their oscillators generate signals of a particular frequency with a random initial phase. The frequency of the generated signal slightly deviates from the targeted frequency owing to the hardware imperfection. This leads to time-varying CFO between the transmitter and receiver. To better characterize how CFO changes over time, we measure the CFO over a period of time through both theoretical analysis and benchmark experiments. We use the signal transmitted from one antenna to estimate the CFO. Specifically, we consider two adjacent chirps transmitted through the same antenna and assuming the CFO does not change during a short period of time such as a chirp

duration (e.g., 10 ms). We denote the phase induced by CFO in the first chirp as $\Phi_{CFO1}(t) = 2\pi\Delta f_c t + \phi_0$, where Δf_c is CFO and ϕ_0 is the initial random phase in the first chirp. As the CFO-induced phase continuously changes, the CFO-induced phase at the end of the first chirp is $2\pi\Delta f_c T + \phi_0$, where T is the chirp duration. Thus, the CFO-induced phase change in the second chirp can be expressed as:

$$\Phi_{CFO2}(t) = 2\pi\Delta f_c t + 2\pi\Delta f_c T + \phi_0 = 2\pi\Delta f_c(t + T) + \phi_0. \quad (11)$$

Therefore, the CFO-induced phase difference between adjacent chirps is $\Delta\Phi_{CFO} = \Phi_{CFO2}(t) - \Phi_{CFO1}(t) = 2\pi\Delta f_c T$. As the chirp period T is known, the value of CFO (Δf_c) can be calculated. We let the LoRa node continuously send four packets from the same antenna. There are 20 chirps in the preamble of each LoRa packet and the chirps in the preamble are complete. We therefore estimate the value of CFO using chirps in the preamble part. As shown in Figure 9, the CFO within each packet gradually decreases with time in a stable way. In a short period of time, e.g., 40 ms, CFO can be safely considered as unchanged. On the other hand, CFO significantly changes between two adjacent packets because the time gap is large and random.

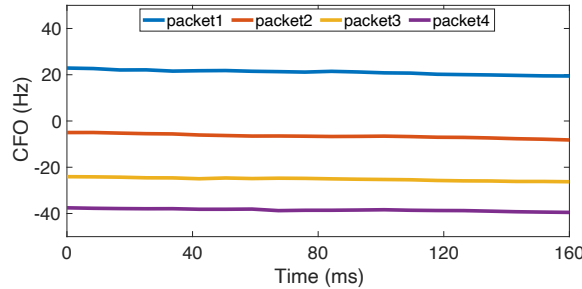


Fig. 9. An illustration of CFO measurement in LoRa packets.

3.3 Antenna Switching Design for LoRa Node

One key issue of controlling the RF switch on LoRa node is to determine when the antenna switching should happen. One simple solution is to switch antenna during the gap between two packets, that is, the first packet is transmitted by antenna Tx1 and the second one is transmitted by antenna Tx2. However, based on the observation in Section 3.2, the CFO significantly changes between two packets. In this case, the phase difference between two packets contains not only the difference of two signal propagation links from two Tx's to Rx, but also the phase difference induced by different CFOs in two packets. While it is easier to cancel the phase offset induced by a constant CFO, it is much more challenging to deal with the phase offset induced by two different random CFOs

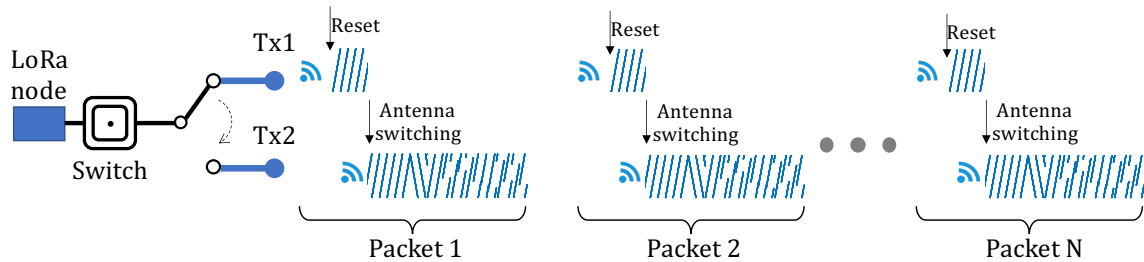


Fig. 10. The workflow of antenna switching design for LoRa node.

in two packets. Therefore, antenna switching must be performed within the transmission of one packet instead of between two packets. Specifically, antenna switching is performed in the preamble of a packet because the preamble contains multiple consecutive complete chirps. Figure 10 shows the workflow of our design. Before one packet is sent, we reset the RF switch to connect to Tx1 and a part of preamble is sent by Tx1. We then control the RF switch to make it connect to Tx2, thus the remaining part of preamble, SFD and payload are sent by Tx2.

3.4 Chirp Ratio Design for Phase Offset Elimination

As introduced in Section 2.3, the phase change of the received signal at LoRa gateway consists of three parts: the phase change of baseband chirp signal, the CFO-induced phase change and the phase change caused by signal propagation. To extract the phase change due to signal propagation which is related to the soil moisture, we propose a chirp ratio approach, which can eliminate the phase change caused by baseband signal and CFO. The key observation to enable this approach is that two adjacent chirps have the same baseband signal phase change. Also the CFO-induced phase changes are very similar since the duration of two chirp is small (e.g., 20 ms) and the CFO changes very little in such a small duration based on the experiment in previous section. Thus, we can use two adjacent chirps to eliminate the phase related to the baseband signal and CFO, and only retain the phase due to signal propagation. We focus on the chirps where antenna switching happens. There are two possible cases: (i) the antenna switching happens within one chirp and (ii) the antenna switching happens at the gap point of two adjacent chirps.

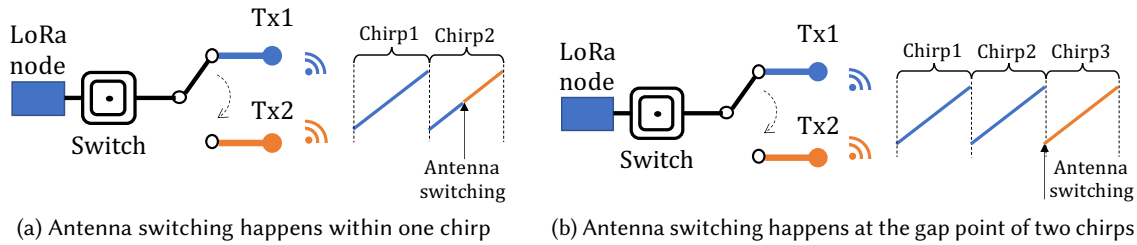


Fig. 11. Two cases of antenna switching.

Case 1: antenna switching happens within one chirp. Let chirp1 denote the last chirp before antenna switching and assume that it is transmitted by Tx1 in Figure 11a. At the receiver, chirp1 can be represented as:

$$R_1(t) = c(t - \tau_1)e^{j(2\pi\Delta f_c t + \Delta\phi_0)} e^{j\Phi_{link1}}, \quad (12)$$

where τ_1 is the time delay of signal propagation from Tx1 to Rx. The phase of $R_1(t)$ is shown in Figure 12b. Then, in the next chirp (chirp2) as shown in Figure 12c, antenna switching happens at timestamp t_s . Note that before t_s , signal still propagates from Tx1 to Rx and the corresponding signal propagation time is still τ_1 . After the antenna switching at t_s , signal propagates from Tx2 to Rx and we denote τ_2 as the signal propagation time of this link. According to the analysis in the previous section, the CFO-induced phase in this chirp is $2\pi\Delta f_c(t + T) + \phi_0$. Thus, the signal of chirp2 at the receiver can be expressed as:

$$R_2(t) = \begin{cases} c(t - \tau_1)e^{j(2\pi\Delta f_c(t+T) + \phi_0)} e^{j\Phi_{link1}}, & 0 < t < t_s \\ c(t - \tau_2)e^{j(2\pi\Delta f_c(t+T) + \phi_0)} e^{j\Phi_{link2}}, & t_s < t < T \end{cases}. \quad (13)$$

Although the phase of the signal has a sudden change at t_s , because the phase of the baseband chirp signal and the CFO-induced phase also change rapidly with time, it is difficult to detect the sudden phase change caused by

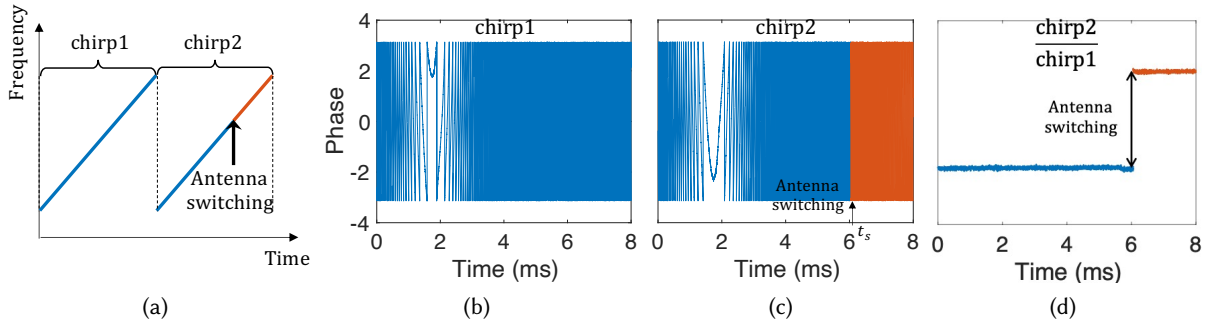


Fig. 12. The illustration of antenna switching case 1: (a) antenna switching happens within one chirp (i.e., chirp2). (b) and (c) The phase of chirp1 and chirp2 change rapidly over time due to the existence of the phase of baseband chirp signal and the CFO-induced phase. The sudden phase change due to antenna switching in the phase of chirp2 can not be detected. (d) The phase of chirp ratio of chirp2 and chirp1. The phase of baseband chirp and the CFO-induced phase are removed so that the phase change induced by antenna switching can be detected easily.

the antenna switching as shown in Figure 12c. To solve this problem, we take the division operation between these two adjacent chirps to obtain the chirp ratio:

$$CR(t) = \frac{R_2(t)}{R_1(t)} = \begin{cases} e^{j2\pi\Delta f_c T} & , 0 < t < t_s \\ \frac{c(t - \tau_2)}{c(t - \tau_1)} e^{j2\pi\Delta f_c T} e^{j(\Phi_{link2} - \Phi_{link1})} & , t_s < t < T \end{cases}. \quad (14)$$

The result of dividing the two chirps is $\frac{c(t-\tau_2)}{c(t-\tau_1)} = \frac{e^{j\pi(k(t-\tau_2)^2-B(t-\tau_2))}}{e^{j\pi(k(t-\tau_1)^2-B(t-\tau_1))}} = e^{j\pi((B-2kt)(\tau_2-\tau_1)+\tau_2^2-\tau_1^2)}$. The magnitude of $B - 2kt$ is on the scale of 10^5 Hz, the magnitudes of τ_1 and τ_2 are on the scale of 10^{-6} s and the magnitude of $\tau_2 - \tau_1$ is on the scale of 10^{-10} s. Thus, $(B - 2kt)(\tau_2 - \tau_1) + \tau_2^2 - \tau_1^2$ can be approximate as zero and $\frac{c(t-\tau_2)}{c(t-\tau_1)} \approx 1$. According to Equation 8, $\Phi_{link2} - \Phi_{link1} = \Delta\Phi$. Thus, the chirp ratio can be simplified as:

$$CR(t) = \begin{cases} e^{j2\pi\Delta f_c T} & , 0 < t < t_s \\ e^{j2\pi\Delta f_c T} e^{j\Delta\Phi} & , t_s < t < T \end{cases}. \quad (15)$$

Figure 12d shows the chirp ratio of chirp2 and chirp1. Compared with the phase of original chirp signal shown in Figure 12c, the phase change at the time of antenna switching due to signal propagation path change can now be clearly extracted. Antenna switching mostly happens within the period of a chirp.

Case 2: antenna switching happens at the gap point of two chirps. It is also possible that the antenna switching happens exactly at the gap point between two chirps as shown in Figure 11b. In this case, the above method fails because the phase of chirp ratio between chirp3 and chirp2 does not change at all, as each chirp has a unchanged propagation path. Besides, when the antenna switching happens at a time close to the chirp gap point, the time interval before or after the sudden change in the chirp is too short that the phase difference is difficult to be accurately extracted due to low sampling rate.

In order to solve this issue, we propose to use three chirps in this case. Assume that both chirp1 and chirp2 are transmitted by Tx1, and the third chirp chirp3 is transmitted by Tx2. The basic observation is that the chirp ratio of chirp2 and chirp1 only contains CFO-induced phase, while the chirp ratio of chirp3 and chirp2 consists of both CFO-induced phase and the phase change caused by the propagation path change. Considering that the CFO has not changed in such a short period of time, the phase of the first chirp ratio, which is the ratio of chirp2 and chirp1 can be used to estimate the CFO. The first chirp ratio can be represented as $CR_1(t) = e^{j2\pi\Delta f_c T}$. The second

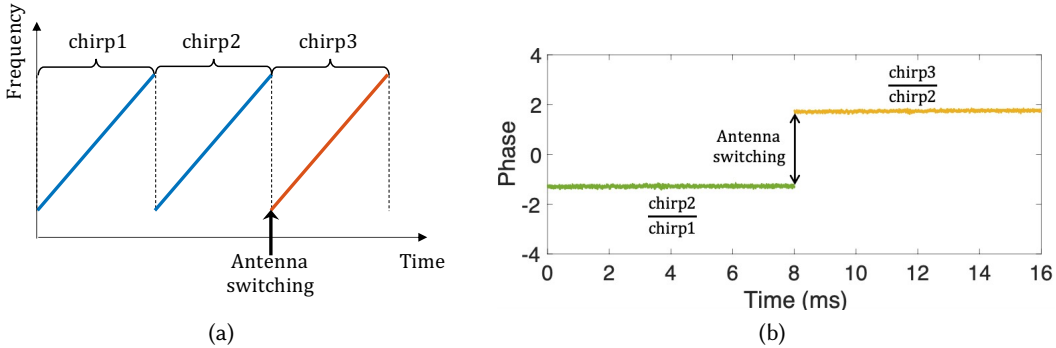


Fig. 13. The illustration of antenna switching case 2: (a) antenna switching happens at the gap point of two chirp (i.e., chirp2 and chirp3). (b) the phase change induced by antenna switching can be measured by calculating the phase difference between the phase of chirp ratio of chirp3 and chirp2 and the phase of chirp ratio of chirp2 and chirp1.

chirp ratio, which is the ratio of chirp3 and chirp2, is $CR_2(t) = e^{j2\pi\Delta f_c T} e^{j\Delta\Phi}$. Therefore, by calculating the phase difference of these two chirp ratios, the phase change $\Delta\Phi$ due to switching can be estimated. Figure 13b shows an example of the phases of two chirp ratios. The difference between them is the phase change due to the signal propagation path change (antenna switching).

Now it has been shown that the baseband signal and CFO-induced phase changes can be eliminated and the phase difference of two signal propagation links can be extracted accurately. Finally, we can calculate the dielectric permittivity based on Equation 9 and estimate soil moisture according to Equation 2.

4 SYSTEM IMPLEMENTATION

4.1 Hardware Implementation

Our LoRa-based soil moisture sensing system consists of multiple LoRa nodes and one gateway. The number of LoRa nodes is determined based on the needs of the scenario, such as the size of the farmland needs to be monitored. The LoRa node is a Semtech SX1276 chip [19] based Dragino LoRa shield [12] controlled by an Arduino Uno. As shown in Figure 14a, each LoRa node is equipped with an HMC849 [16] single-port-dual-throw (SPDT) RF switch, which is controlled by the same Arduino Uno through GPIO ports. The unit cost of the HMC849 SPDT RF switch is \$3.75 [15]. Two antennas are connected to the SPDT RF switch. LoRa node transmits signals at

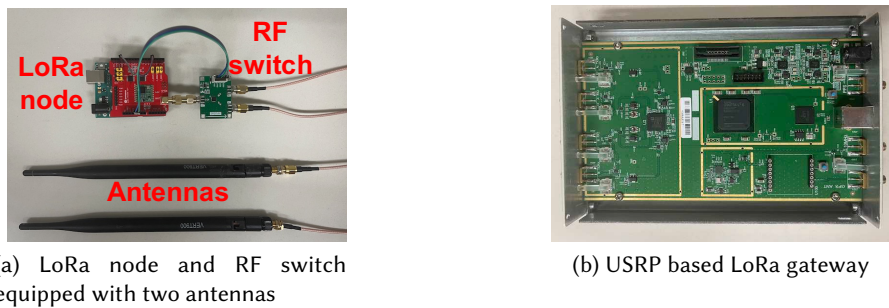


Fig. 14. Hardware of our system.

the 915 MHz frequency with a bandwidth of 125 kHz. The chirp duration is set to 8 ms. The LoRa gateway is implemented on USRP B210 [21] as shown in Figure 14b. The LoRa gateway is connected to a laptop with an Intel Core i7 CPU and 16 GB RAM. It collects data at a rate of 1 MHz and processes them using MATLAB in real time.

4.2 Software Implementation

Figure 15 illustrates the proposed soil moisture sensing process. It consists of four core modules: (1) data acquisition, (2) signal preprocessing, (3) phase offset elimination and (4) soil moisture estimation.

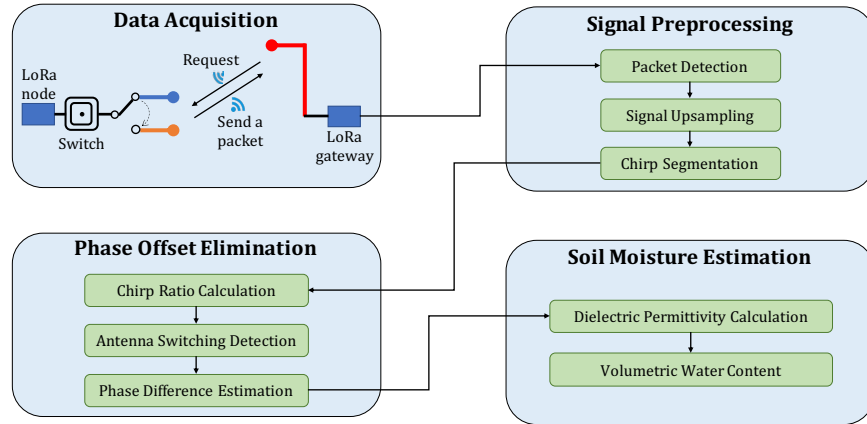


Fig. 15. Soil moisture sensing system overview.

4.2.1 Data Acquisition. In our system, LoRa node only sends one packet when a node receives a soil moisture measurement request from the LoRa gateway. When LoRa node is not sending packets, it is in the sleep mode. This design has two benefits. The first one is to save power as LoRa nodes are usually battery-powered. The second one is that multiple LoRa nodes can avoid sending packets at the same time which may cause collisions at the gateway. Since the duration of a LoRa packet is very short (e.g., less than 1s), the system does not need to use concurrent measurements to save time, because soil moisture does not change in a short period of time. For LoRa nodes, we set signal parameters and control signal transmission by an open source C library [4]. The antenna switching timestamp is set to be within the preamble. This is feasible because the number of chirps in the preamble and the duration of a chirp are standardized and therefore are known. Each time before one packet is sent, RF switch is connected to port1 and a few chirps in the preamble are transmitted by Tx1. Then the RF switch is connected to port2 and the remaining preamble, SFD, and payload are sent through Tx2. For LoRa gateway, we use the free GNURadio software [14] to control the USRP to receive LoRa signal samples. The raw data are processed using MATLAB.

4.2.2 Signal Preprocessing. In this module, we show how to detect the beginning of a LoRa packet in the received signal. We use the energy threshold based method to detect the arrival of LoRa packets. That is, we utilize signals collected during the time of no packet transmission to determine the noise floor in the current environment. After that, the LoRa gateway sends a measurement request and waits for the arrival of the reply. We then continuously check whether the channel energy is higher than the noise floor by a threshold (i.e., 3 dB in our design). If it is, a packet arrival is detected. We can also detect the end of the packet based on the noise floor. In this way, the signal of a complete packet can be extracted. Next, we need to determine the number of samples inside a chirp,

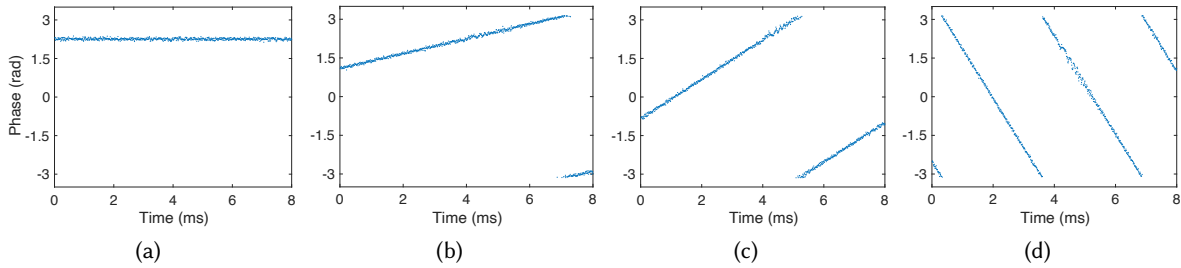


Fig. 16. Examples of the division of two windows. (a) shows when the two windows are aligned, the phase of the division of them is stable. (b), (c) and (d) show the examples of the division of two misaligned windows, and the more misaligned the two windows, the more obvious the phase change over time.

so as to accurately segment each chirp to prepare for the calculation of chirp ratio. We select the first M samples of a packet as the first window. Then we slide forward to create a new window with M samples, and divide each window by the first window.

The basic idea behind here is that if the window is moved to the same position in the second chirp (i.e., aligned), the division will bring us a constant phase as shown in Figure 16a, since the common baseband signal phase change and CFO-induced phase change are removed. In this case, the distance between the two windows is exactly the length of one chirp. Note that when we move the window, the step size determines the search speed. When the distance between the two windows does not match the chirp length, the phase still changes with time as shown in Figure 16b, 16c and 16d. The more closer we get the correct distance, the smaller the slope of phase is. We therefore employ a binary search here which can quickly converge to the correct distance by checking if the division presents us a smaller slope.

However, we find in practice it is difficult to find such a distance that makes phase difference be a constant. After we dig deeper, we find that this is due to the effect of sampling time offset between adjacent chirps. An intuitive explanation is shown in Figure 17a. The timestamp of the first sample in the first chirp is t_1 , and the timestamp of the first sample in the second chirp is t_2 . Therefore, the two chirps can never be aligned at this coarse sampling interval. To solve this problem, we upsample the received signal, i.e., interpolate the received signal. In this way, the number of samples in each chirp increases, and there is a higher chance to find a sample so that the two chirps can be aligned as shown in Figure 17b. From our experiments, upsampling the raw signal from 1 MHz to 10 MHz can make two chirps well aligned. In this way, the length of a chirp can be estimated and then all chirps can be segmented. After that, these chirps can be used to extract the phase of chirp ratio.

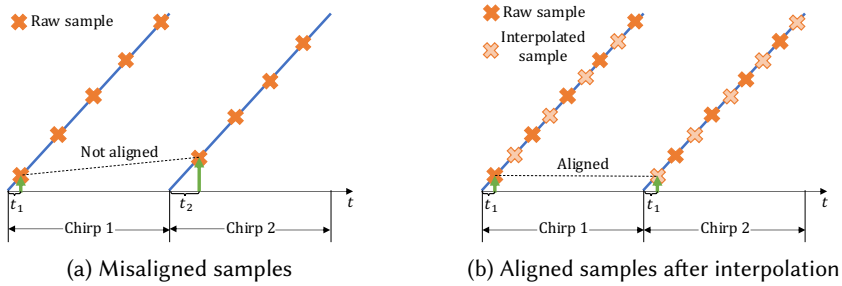


Fig. 17. An illustration of the effect of sampling time offset and upsampling.

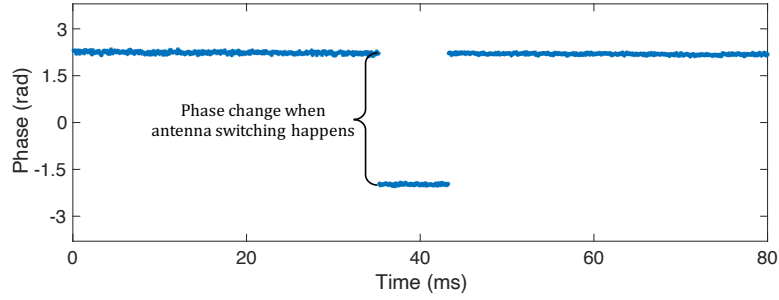


Fig. 18. The phase change when antenna switching happens.

4.2.3 Phase Offset Elimination. At the receiver side, we need to detect the timestamp the antenna switching happens. Since the duration of a chirp has been estimated, all chirps in the preamble can be extracted. The basic idea of antenna switching detection is that if the antenna does not switch, only the CFO-induced component is included in the phase of the ratio of the two chirps. On the contrary, antenna switching will induce a sudden change in the phase due to the propagation link change. Therefore, we calculate the ratio of all two adjacent chirps in the preamble and extract the phase change. As shown in Figure 18 with real collected data, it is obvious that one of the chirp ratios has a sudden phase change, indicating the occurrence of antenna switching. We calculate the phase change value at the time that the switching happens to get the phase difference of the two signal propagation links.

4.2.4 Soil Moisture Estimation. At last, we estimate the dielectric permittivity of soil. As the example shown in Figure 18, the phase change when antenna switching happens is 4.5. According to Equation 9, the dielectric permittivity is 22.1 when the antenna spacing is 5 cm. Then we compute the soil moisture based on Equation 2, which is 37.0%.

5 EVALUATION

In this section, we evaluate the performance of our system in both laboratory and farmland fields. For laboratory experiments, we first evaluate the overall accuracy of the system at different soil moisture levels and compare the

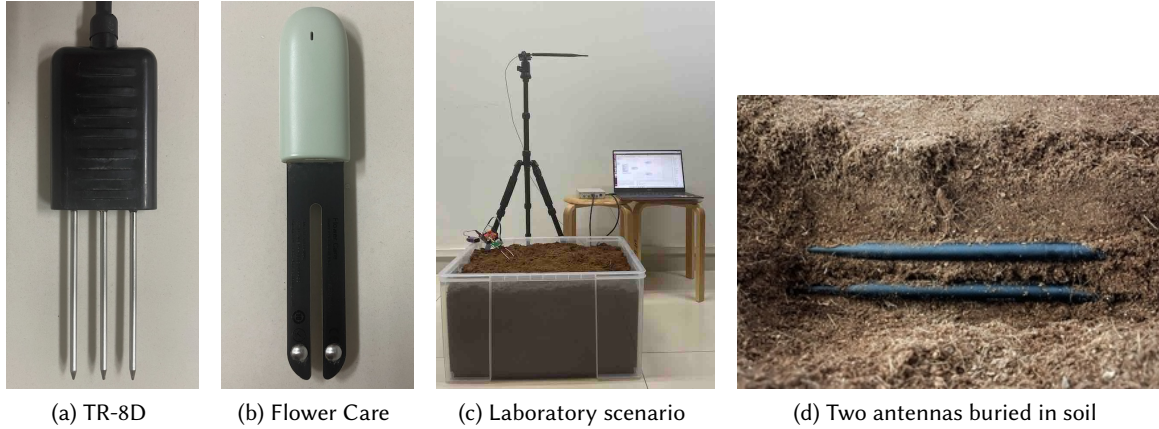


Fig. 19. Laboratory experiments setup.

results with two commodity soil moisture sensors on the market. Then, we evaluate the factors affecting soil moisture sensing including soil type, antenna spacing, antenna depth and the angle between the transceivers. In real-world farmland experiments, we explore the longest distance between the LoRa gateway and LoRa node that the system can still monitor soil moisture and the impact of interference.

Metric: We use the mean absolute error between the estimated soil moisture and the groundtruth as the performance metric. In laboratory experiments, we precisely control the amount of water added to the soil, and use the ratio of the volume of water to the total volume of water and soil as the groundtruth, which is also the definition of soil moisture content. In farmland experiments, since we can not determine the total volume of soil and water after adding water to the soil, we use the soil moisture measured by a high-end dedicated sensor as the groundtruth. Two commodity soil moisture sensors are used in our experiments. As shown in Figure 19a and 19b, the two sensors are TR-8D [20] which costs \$400 and HHCC Flower Care [13] which costs \$10, respectively.

Setup: Figure 19c shows the deployment scenario of our system. The two antennas of LoRa node are buried in the soil as shown in Figure 19d, and the spacing between the two antennas is 4 cm. The antenna of the LoRa gateway is placed one meter above the soil surface.

5.1 Overall Performance

We first evaluate the overall performance of our system using one type of soil, i.e., loam soil. Figure 19c shows the setup of our laboratory experiments. We use a $60\text{cm} \times 50\text{cm} \times 40\text{cm}$ rectangular plastic box as the container for soil. We place the two antennas of the LoRa node 10 cm below the soil surface, and the antenna spacing is 4 cm. The antenna of the LoRa gateway is placed 1 m above the soil surface. Starting from the driest soil, we add water to the soil ten times and calculate the groundtruth of soil moisture. Figure 20 shows the soil under three

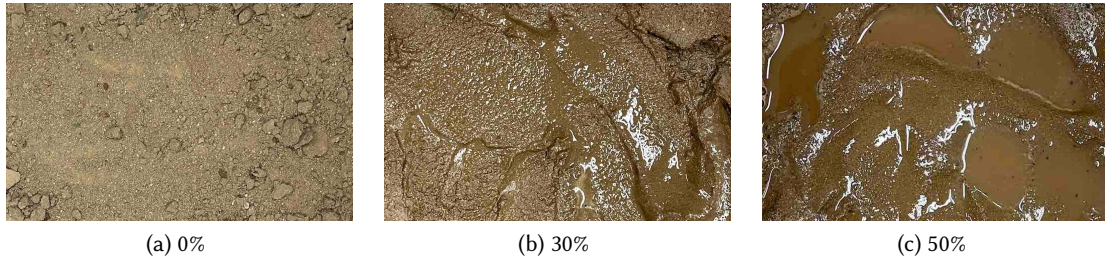


Fig. 20. Soil under different moisture levels.

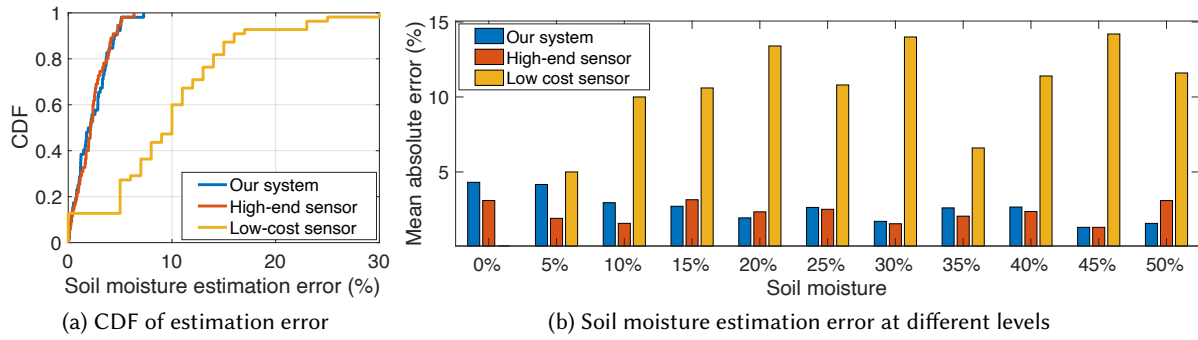


Fig. 21. Overall performance.

different moisture levels including 0%, 30% and 50%. During the process of measuring soil moisture using our LoRa-based system, we also record the measurement results of two dedicated sensors. As shown in Figure 21a, the 90-percentile estimation error of the proposed LoRa-based system and two sensors are 4.4%, 4.3% and 17.2%, respectively. This result shows that the accuracy of our system is much higher than that of the low-cost sensor and is comparable to that of the high-end sensor which costs \$400. Figure 21b shows the accuracy of our system and sensors at different soil moisture levels. The mean absolute error of our system in various soil moisture levels is 3.1% and there is no obvious difference under different moisture levels, which means that our system can work under various soil moisture levels. Note that our system can still work when the absolute soil moisture is higher than 50%. However, in these scenarios, the water and soil actually become two separate layers.

5.2 Impact of Different Factors

5.2.1 Impact of Antenna Spacing. In real-world settings, the antenna spacing of the LoRa node is very important. In general, the maximum volumetric water content of the soil is about 50% [10, 25, 41], and the dielectric permittivity of the soil is 40 [42]. In order to avoid the phase ambiguity issue, the signal phase difference between the two antennas should be smaller than 2π when the soil moisture reaches the maximum. According to Equation 8, we should set antenna spacing smaller than 5.2 cm. To demonstrate the necessity of meeting this antenna spacing requirement in real-world setting, we conduct a benchmark experiment to verify the phase difference between two antennas when the antenna spacing is greater than 5.2 cm. We conduct three sets of experiments with the antenna spacing set as 5 cm, 6 cm and 7 cm, respectively. For each antenna spacing, we test five soil moisture levels. As shown in Figure 22a, when the antenna spacing is 5 cm, as the soil moisture increases, the phase difference between the two antenna signals gradually increases. When the moisture is 50%, the phase difference is close to 2π . However, when the antenna spacing is 6 cm and 7 cm, and the moisture is 50% and 40%, the phase difference has exceeded 2π and is wrapped within 0 and 2π , which causes the issue of phase ambiguity. If we employ the wrapped phase for soil moisture estimation, the soil moisture will be wrongly estimated. Therefore, the antenna spacing must be set below 5.2 cm to avoid the phase ambiguity. We then vary the antenna spacing from 1 cm to 5 cm at a step size of 1 cm to evaluate the sensing performance. Five soil moisture levels are considered for each antenna spacing. Figure 22b shows that the average moisture error is less than 4% when the antenna spacing is between 2 cm and 5 cm. However, when the antenna spacing is 1 cm, the error increases to 7.8%. We believe this is due to antenna coupling when two antennas are placed too close to each other.

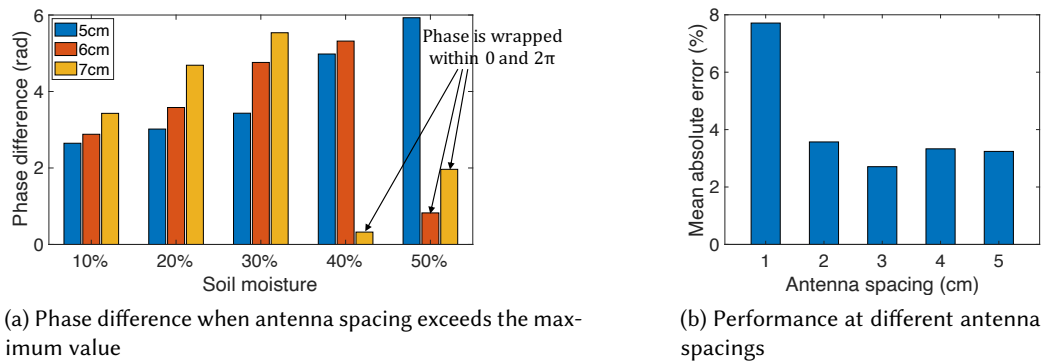


Fig. 22. Impact of antenna spacing.

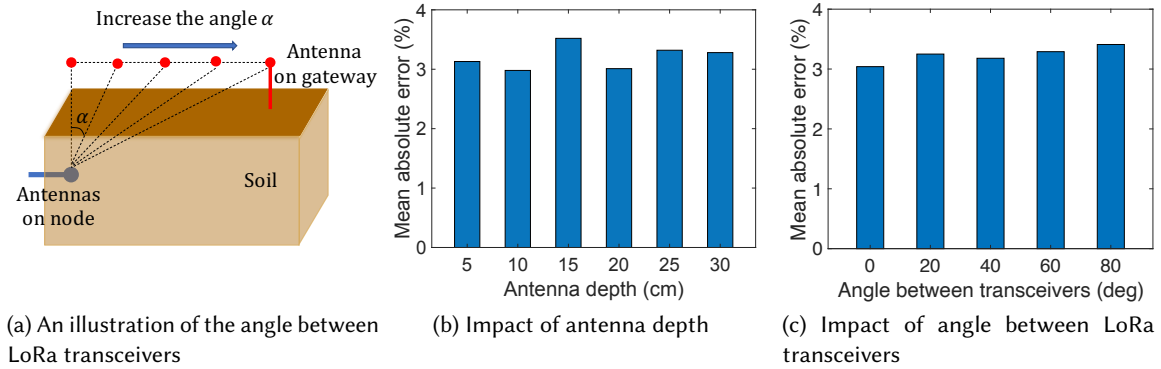


Fig. 23. Impact of different factors.

5.2.2 Impact of Antenna Depth. The antenna depth (i.e., the distance between soil surface and the upper antenna) is an important parameter for soil moisture measurement. For dedicated sensors, they are generally buried in the depth of the soil where the moisture needs to be measured. We conduct experiments to verify the accuracy of our system at different depths. We vary the antenna depth from 5 cm to 30 cm at a step size of 5 cm. At each depth, we test five different soil moisture levels. As shown in Figure 23b, at various depths, the average errors of our system are always less than 3.5%, indicating that our system can work at various depths.

5.2.3 Impact of Angle between LoRa Transceivers. Next, we conduct experiments to verify the accuracy of soil moisture measurement under different transmitter-receiver angles. As illustrated in Figure 23a, we change the angle α between LoRa transceivers from 0° to 80° at a step size of 20° . As shown in Figure 23c, the mean absolute errors of the system at various angles are always less than 3.6%. We do observe slightly increasing errors when the angle increases.

5.2.4 Impact of Soil Type. In real world, there are many types of soil. We conduct experiments to evaluate the performance of the system with different types of soils. As shown in Figure 24, we select five common types of soil, which are sandy soil, loam, loess, red clay and coir soil. For each soil, we measure the soil moisture at five moisture levels. Figure 24f shows the average measurement error for each type of soil. It can be observed that our system can achieve high accuracy for all soil types and there is no obvious performance difference between

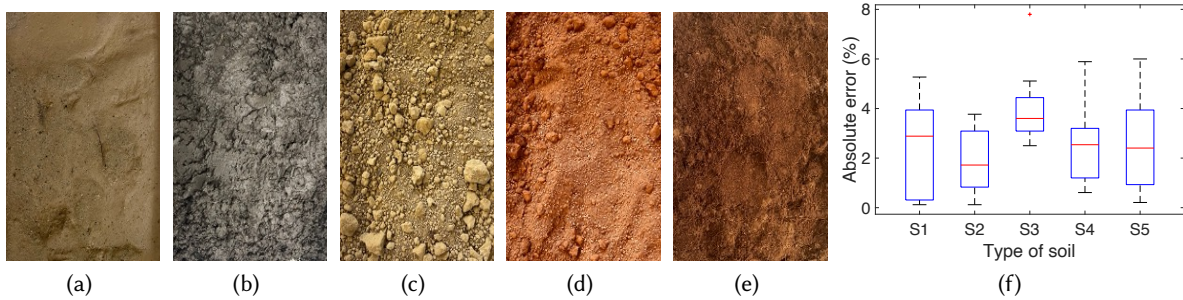


Fig. 24. Impact of different types of soil. (a) S1: sandy soil. (b) S2: loam. (c) S3: loess. (d) S4: red clay. (e) S5: coir soil. (f) The performance in different types of soil.

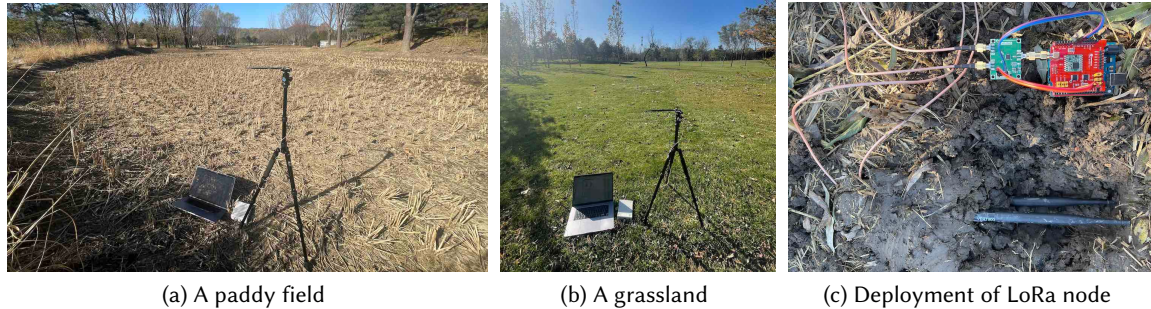


Fig. 25. Field study scenario and setup.

different soil types. Furthermore, in our experiments, different soils have different densities. We also add different amounts of water to each soil type, which cause the density of the soil to change. The results show that our system can achieve high accuracy in all the cases, which demonstrate the density of the soil does not affect the performance of our system.

5.3 Field Experiments

We deploy our proposed system at a paddy field and a grassland as shown in Figure 25. Figure 25c shows the detailed deployment of the LoRa node in our system. The antennas are placed 5 cm below the soil and the antenna spacing is set as 3 cm. The antenna of the LoRa gateway is placed 1.5 m above the ground.

5.3.1 Verification of the Support of Multi-node Measurement. We first verify the soil moisture measurement error of the system in the paddy field shown in Figure 25a. We deploy a total of six nodes in the paddy field with a size of $30\text{ m} \times 30\text{ m}$. The distance from the nodes to the gateway ranges from 5 m to 30 m. We use the high-end soil moisture sensor to measure the groundtruth soil moisture. As shown in Figure 26, when the distance between node and gateway increases, the system error slightly increases. However, even at a distance of 30 m, the system error is only increased from 3.6% to 4.9% compared with that at a distance of 5 m. This result shows the accuracy of our system in a real agricultural scenario.

While measuring the soil moisture, we also evaluate the communication performance of the system. Every time we let the LoRa node send a packet to the gateway to measure soil moisture, we also encode data in the packet. At the LoRa gateway, the accuracy of data decoding is always 100%. This shows that the antenna switching design in our system does not interrupt the data communication of LoRa.

5.3.2 Exploring the Longest Distance between LoRa Transceivers. Next, we explore the coverage range of a LoRa gateway for sensing, i.e., the longest distance between the LoRa node and gateway the soil moisture system can still work. This is important because a larger range can enable the LoRa gateway to cover a larger sensing area, reducing the number of required LoRa gateways² which is critical for large-scale deployment. We conduct experiments in the grassland with a size $30\text{ m} \times 100\text{ m}$ as shown in Figure 25b. We start from 20 m and gradually increase the distance between the LoRa node and the gateway at a step size of 20 m until the signal becomes too weak to be utilized for accurate moisture sensing. We evaluate the sensing range under five different soil moisture levels. In the environment we tested, the soil has a maximum moisture of about 35%. We define the longest sensing distance as the distance with a mean estimation error smaller than 15%. We find that the longest sensing working distance is about 100 m. Figure 27 shows the estimation error at each distance. When the distance reaches

²The LoRa gateway is much more expensive than the LoRa node.

100 m, the error is 13%. This result shows the accuracy and robustness of our system in real-world scenarios and demonstrates the possibility of employing the proposed system for large-scale deployment in farmland to help achieve the goal of precision irrigation.

5.3.3 Soil Moisture Estimation at Different Depths. It is known that the soil moisture changes as the soil depth increases [2]. On the other hand, different crops have different root depths, so the depth at which soil moisture needs to be monitored varies with crops. To show our system can measure soil moisture at different depths in real world scenarios, we measure soil moisture at different depths in the grassland. As shown in Figure 28a, we measure the soil moisture at the depth from 5 cm to 30 cm at a step size of 5 cm. The groundtruth is measured by the high-end soil moisture sensor. We set the antenna spacing as 3 cm, and measure the soil moisture at six depths. As shown in Figure 28b, the soil moisture first increases from 11% to 25%. After that, from 20cm to 30cm, the soil moisture was reduced from 25% to 16%. This shows that the soil moisture changes with the soil depth in real-world scenarios.

5.3.4 Impact of Antenna Angle. In real-world deployment, the antennas may not always be placed in parallel with the ground surface. In this experiment, we evaluate the effect of antenna angle on sensing performance. As shown in Figure 29a, the antenna angle β is defined as the angle between the antenna and the horizontal plane. The antenna spacing is the distance between the two antennas in the vertical direction. We vary the antenna angle from 0° to 90° . As the results shown in Figure 29b, when the antenna angle is less than 60° , the soil moisture estimation error is less than 6.4%. The error increases to 20% when the antenna angle is 90° which is perpendicular

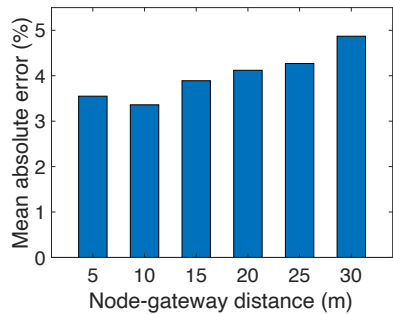


Fig. 26. The accuracy of different nodes in a paddy field.

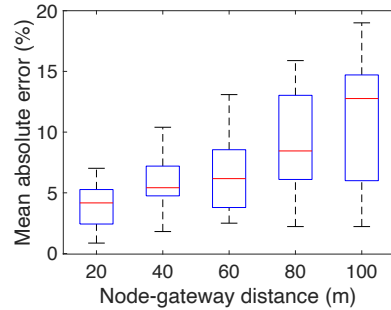
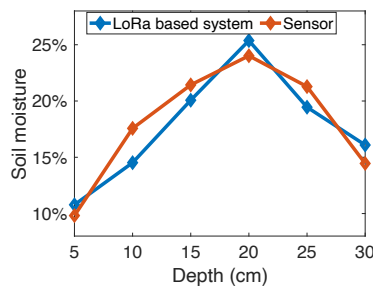


Fig. 27. Exploring the longest distance.



(a) A pit dug for experiment



(b) Soil moisture at different depths

Fig. 28. The impact of moisture changing with soil depth.

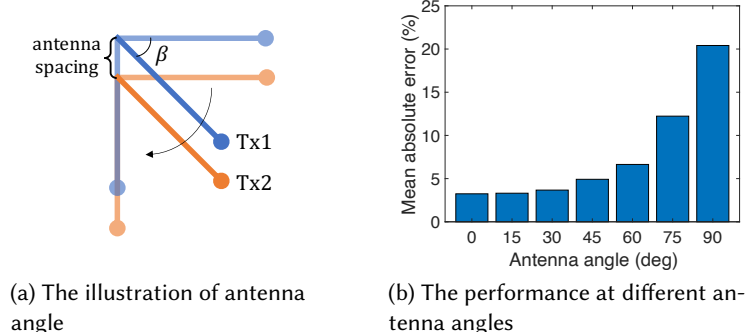


Fig. 29. The impact of antenna angle.

to the surface ground. We believe the increased error is due to the varying soil moisture at different depths. When we place the antennas vertically in the soil (90°), the LoRa signals are actually measuring the soil moisture in a depth range, causing larger errors.

5.3.5 Impact of Soil Surface Condition. During our experiments, we find that the soil surface condition, i.e., stones on top of the ground surface can affect the sensing performance. In Figure 30a-30e, we show different stone coverage on the soil surface, which are no stones (C1), stones (C2), more stones which can cover the entire surface above the antennas (C3) and a big stone (C4). We also move the big stone in C4 a little bit so that it does not block the signal between the node and gateway (C5). In order to visually show the size of the stones, we place a bottle cap with a diameter of 3 cm near the stones. For each surface condition, the LoRa antennas are buried 20 cm below the surface. The results are shown in Figure 30f. If there are no stones, the grass on the surface does not affect the system performance while the stones (C2) do slightly increase the measurement error, which is still below 5%. However, if the small stones cover the whole surface above the antennas, the system error increases to 10%. If a big stone is right above the antennas, the error is about 18%. However, if we move the big stone a little bit to make sure it does not block the propagation path, the error is decreased to below 4%. These results show the robustness of our system in real-world environment. The reason the stones affect the sensing performance is that the phase difference of the two links is now not just affected by the soil moisture but also the stones.

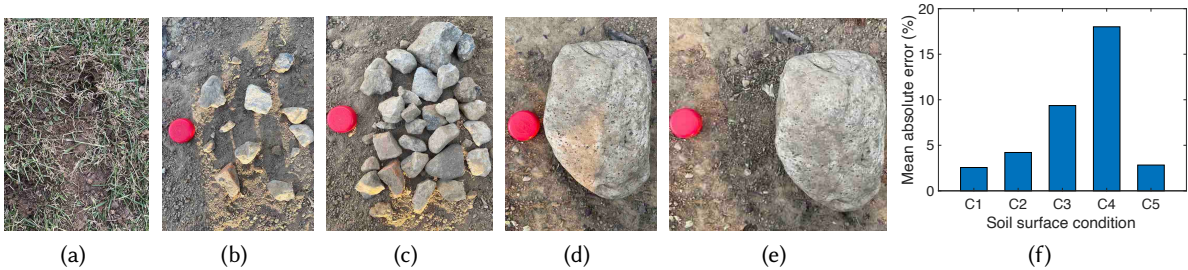


Fig. 30. Impact of different soil surface conditions. (a) C1: no stones. (b) C2: stones. (c) C3: more stones which can cover the entire surface above antennas. (d) C4: a big stone. (e) C5: move the big stone in C4 a little bit so that it does not block the signal. (f) The performance under different soil surface conditions.

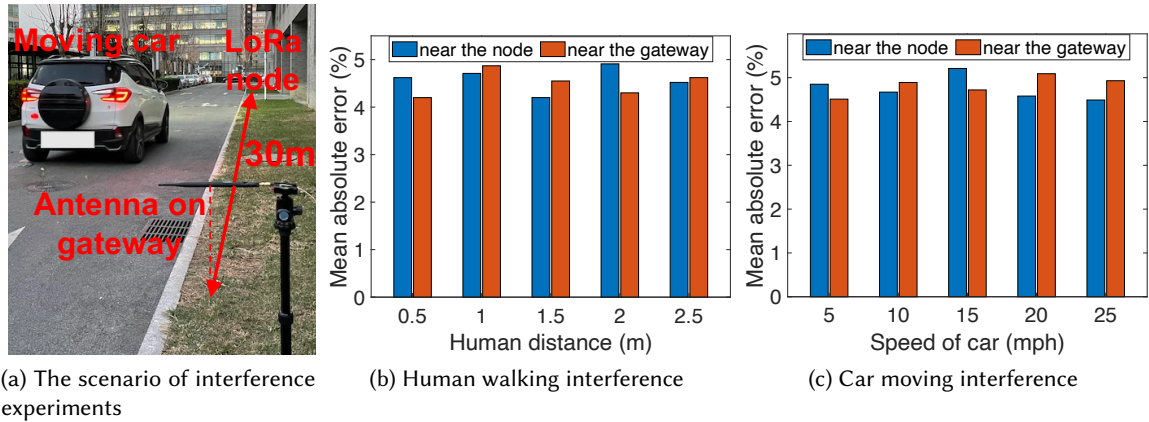


Fig. 31. The impact of motion interference.

5.3.6 Impact of Motion Interference. In addition, to verify the robustness of our system, we evaluate the achieved accuracy when there is motion interference (multipath) near the LoRa node and gateway. We consider two different types of motion interference, i.e., human walking interference and machine moving interference. In these experiments, the distance between LoRa node and gateway is 30 m as shown in Figure 31a. We let one person walk around the LoRa node and the distance between the person and LoRa node is increased from 0.5 m to 2.5 m at a step size of 0.5 m. As shown in Figure 31b, in all scenarios, the human walking interference does not affect the accuracy of soil moisture sensing. We also ask the person to walk around the LoRa gateway and achieve similar performance.

We further consider machine interference. In farmland, there may be agricultural machinery, such as seed drills and reapers moving around. In order to simulate the impact of these machinery passing by the LoRa node or gateway, we let a car pass by the LoRa gateway with a short distance of 1 m between the car and the LoRa gateway. We also let a car pass by the LoRa node at the same distance. We let the car move at five different speeds ranging from 5 mph to 25 mph. The results are shown in Figure 31c. We can see that the soil moisture estimation error remains under 5% for all scenarios. We believe the main reason which makes our system robust against interference is that in our system, the phase change used for moisture sensing is through antenna switching which happens in a very short period of time. Through our experiment, the sudden phase change takes about 10 μ s to complete. In such a short period of time, the interferer only moves very little (less than 0.2 mm), and the phase change induced by the interferer can be safely neglected.

6 RELATED WORK

Soil moisture sensing. Several commercial sensors have been used to sense soil moisture by measuring the properties of soil which are closely related to the moisture, including capacitance sensors [57] [62] [46] [49] [32] [28], electrical resistance sensors [53] [35] [29], tensiometers [27], and neutron probe [34] [23] [69]. These sensors are often very expensive and cannot obtain high measurement accuracy in all types of soil. For example, in high-salinity soils, capacitance sensors will falsely overestimate soil moisture [7]. There are also some sensors that use the characteristics of RF signals in the soil to measure soil moisture. Hilhorst *et al.* [40] propose Frequency Domain Reflectometry (FDR) based sensors, which measure the frequency change of RF signal in soil induced by moisture change. The cost of FDR-based sensors can be low (i.e., \$5-\$50) [38]. However, the accuracy is low since they are easily affected by soil type, salinity and temperature [55]. Topp *et al.* [63] propose Time Domain

Reflectometry (TDR) based sensors to calculate the propagation speed of the RF signal in soil by measuring the Time of Flight (ToF) of RF signal at the probes inserted into the soil, and then estimate the soil moisture. However, to achieve highly accurate time measurement, expensive high-end oscillator is required which leads to high cost of the moisture sensor. The high cost (the cost of sensor is more than \$250 and the cost of data logger is more than \$1000 [8]) limits the large-scale use of them in agriculture [38].

Besides the sensor based soil moisture sensing, researchers also explore RF signal to estimate soil moisture. Remote sensing [68] [43] is an early RF technology used to sense soil moisture which utilizes the reflection properties of the soil surface to the RF signal. This method can obtain soil moisture information in a coarse-grained regional level which is too coarse for smart agriculture. Ground Penetrating Radar (GPR) [33] [47] is a non-invasive soil moisture sensing method, which estimates the signal propagation speed by accurately measuring the ToF of a large bandwidth signal in the soil. Although GPR can achieve very high accuracy, its extremely high cost (\$14000 [6]) and inconvenience make it unsuitable to be widely used. In recent years, researchers explore soil moisture sensing based on ubiquitous wireless signals, such as RFID and WiFi signals. RFID based approaches [24] [22] [61] [67] are based on the principle that the signal has different amount of attenuations in soils with different moisture levels. Although the deployment is relatively simple, the coarse-grained accuracy and short sensing distance are still key limitations. Ding *et al.* [30] propose to sense soil moisture accurately using WiFi signal. However, the communication range of WiFi is around 50-100 m while the sensing range is much smaller, i.e., 5-10 m. The WiFi based soil moisture sensing range reported in [30] is merely 1 m. WiFi infrastructure is also mostly deployed in indoor environments and is not available in smart agriculture scenarios. Furthermore, the transmission power of WiFi is typically 100 mW, which is also much higher than that of LoRa (20 mW). In this work, we propose to sense soil moisture using LoRa signal, which has already been widely used in smart agriculture.

LoRa-based communication and sensing. LoRa is a promising communication technology with low power consumption, long range, and high-reliability properties [48]. Traditional LoRa research mainly focuses on long-distance IoT data communication. LoRa technologies have been applied in many application scenarios such as smart agriculture [73][59], environment monitoring [52] [39], facility management [58], intelligent building control [45], vehicle tracking [37], and smart industry [18][56]. Zhao *et al.* [76] propose to utilize a sensing platform with LoRa radios to monitor air quality. Mathur *et al.* [37] utilize LoRaWAN to enable crowdsourced traffic calming and traffic sensing. They propose an adaptive data aggregation and re-transmission scheme for relaying traffic data from sensors. Specifically, Van *et al.* [66] deploy LoRa nodes for greenhouse agriculture and transfer collected sensor data of soil moisture. Sensoterra [5] is a wireless and self-sustaining soil moisture measurement system, which uses LoRa to transmit data collected from dedicated sensors. All these works only employ LoRa transceivers to transfer collected sensor data. Recently, LoRa-based localization has gained some interests. Lin *et al.* [50] study the feasibility of LoRa-based localization, which shows a phase-based localization approach outperforms RSSI-based and TDoA-based approaches. Liu *et al.* [51] propose a system to achieve high accuracy in both indoor and outdoor localization. Rajalakshmi *et al.* [54] develop a multi-band LoRa backscatter system for localization and achieve a range up to 60 m. Researchers also propose to use LoRa to achieve long-range through-wall wireless sensing. Zhang *et al.* [74] utilize LoRa to realize breathing monitoring and walking distance estimation of people at 30 m, and further design a LoRa beamforming technique to support multi-target sensing [75]. Chen *et al.* [26] and Xie *et al.* [71] study how to eliminate irrelevant interference in the environment while utilizing LoRa signals for long-range sensing. Xie *et al.* [72] further push the sensing range of human walking and respiration monitoring to 120 m and 75 m, respectively using LoRa signals.

7 DISCUSSION

In this section, we discuss possible concerns, limitations and potential future work.

Joint soil moisture sensing and data communication. The experiment results in Section 5.3.1 show that in our deployment, the data communication of LoRa is not interrupted by the soil moisture sensing, although one LoRa packet is separately transmitted by two antennas due to antenna switching (Section 3.3). We also want to point out that the proposed system just requires a small part (preamble) of one packet to complete the task of moisture sensing. Also the proposed system does not need to transmit any dedicated packets. Any packet from LoRa node can be utilized for sensing.

Enlarging the sensing range with the help of UAVs. Comprehensive experiments have verified that the proposed system can accurately measure soil moisture even when the LoRa gateway is 100 m away from the node. However, the size of a farmland in agriculture can be on the scale of tens of kilometers. We envision the LoRa gateway to be placed on Unmanned Aerial Vehicles (UAVs) to further increase the sensing coverage.

Application of the CFO elimination scheme to other applications. We propose a chirp ratio based method for CFO estimation and elimination. The basic idea of this approach is that adjacent LoRa packets have similar CFOs. This is a general CFO cancellation scheme which can be applied to any applications that require multiple antennas at the transmitter to transmit chirp signals to a common receiver.

Limitation. For long-term sensing, the roots of plants in the ground may block the signal. In addition, stems and leaves of huge plants above the ground may also affect signal propagation. These are very important issues we will deal with in our future work to move our system one step further towards real-life adoption.

8 CONCLUSION

In this paper, we propose a LoRa signal based system that measures soil moisture without requiring any dedicated sensors in the soil. The key technical novelty of our design lies in using a low-cost RF switch to create signal propagation path length difference for accurate moisture sensing. We study the theoretical relationships between LoRa signal phase change and soil moisture and develop a chirp ratio approach to extract fine-grained phase information for sensing. We evaluated the proposed system in both indoor and outdoor environments. We demonstrate a large 100 m moisture sensing range of LoRa, which is promising for potential large-scale deployment. With the switch design, our system can resist interference from walking people and moving vehicles, paving the way for real-world deployment of soil moisture sensing using LoRa signals.

ACKNOWLEDGMENTS

This work is partially supported by the National Natural Science Foundation of China (No.62172394, No. 62072450), the National Natural Science Foundation of China A3 Foresight Program (No.62061146001), the Youth Innovation Promotion Association, Chinese Academy of Sciences (No. 2020109), the EU CHIST-ERA RadioSense Project, the EU Horizon 2020 research and innovation programme IDEA-FAST (No. 853981) and the National Key Research and Development Plan (2020YFB2103900).

REFERENCES

- [1] 1993. *Water Resource Issues and Agriculture*. <https://www.fao.org/3/t0800e/t0800e0a.htm>
- [2] 2013. *Practical Use of Soil Moisture Sensors and Their Data for Irrigation Scheduling*. <http://irrigation.wsu.edu/Content/Fact-Sheets/FS083E.pdf>
- [3] 2017. *Review of latest developments in the Internet of Things*. https://www.ofcom.org.uk/__data/assets/pdf_file/0007/102004/Review-of-latest-developments-in-the-Internet-of-Things.pdf
- [4] 2018. *MQTT over LoRA*. <https://github.com/bngesp/MQTT over LoRA/tree/adcf780d5e85f0cb6e030cc0d1f97795b8bb7a10/SX1276>
- [5] 2018. *Semtech, Senet and Sensoterra's Proven IoT Solution for Farmers*. <https://www.semtech.com/company/press/semtech-senet-and-sensoterras-proven-iot-solution-offers-farmers-scale-and-operational-visibility>
- [6] 2019. *Ground Penetrating Radar Cost*. <https://usradar.com/ground-penetrating-radar-cost/>
- [7] 2019. *Soil moisture monitoring: a selection guide*. <https://www.agric.wa.gov.au/horticulture/soil-moisture-monitoring-selection-guide>

- [8] 2019. *Soil moisture sensors for irrigation scheduling*. <https://extension.umn.edu/irrigation/soil-moisture-sensors-irrigation-scheduling#electrical-resistance-sensors-1870361>
- [9] 2020. *Requirements for Uniform Germination and Emergence of Corn*. <https://www.agry.purdue.edu/ext/corn/news/timeless/germemergreq.html>.
- [10] 2020. *Soil moisture - Carbon tree*. <http://www.hiilipuu.fi/articles/soil-moisture>.
- [11] 2020. *Water in Agriculture*. <https://www.worldbank.org/en/topic/water-in-agriculture#1>
- [12] 2021. *Dragino LoRa shield*. <http://www.dragino.com/products/module/item/102-lora-shield.html>
- [13] 2021. *Flower Care Smart Monitor*. <http://www.huahuacaocao.com/product>
- [14] 2021. *GNURadio*. <https://www.gnuradio.org/>
- [15] 2021. *HMC849A*. <https://www.analog.com/en/products/hmc849a.html#product-samplebuy>
- [16] 2021. *HMC849ALP4CE RF Switch*. <https://www.analog.com/media/en/technical-documentation/data-sheets/hmc849a.pdf>
- [17] 2021. *Moisture Measurement with the Bluelab Pulse Meter*. <https://support.bluelab.com/hc/en-us/articles/36000492455-moisture-measurement-with-the-bluelab-pulse-meter>.
- [18] 2021. *Semtech*. <https://www.semtech.com/lora/lora-applications>, WhitePaper.
- [19] 2021. *Semtech SX1276 Transceiver*. <https://www.semtech.com/products/wireless-rf/lora-transceivers/sx1276>
- [20] 2021. *TR-8D*. <https://www.yoycart.com/Product/603349297432/>
- [21] 2021. *USRP B210*. <https://www.ettus.com/all-products/ub210-kit/>
- [22] Rafael V. Aroca, André C. Hernandes, Daniel V. Magalhes, Marcelo Becker, and Adonai G. Calbo. 2018. Calibration of Passive UHF RFID Tags Using Neural Networks to Measure Soil Moisture. *Journal of Sensors* 2018 (2018), 1–12.
- [23] Chm Van Bavel, N. Underwood, and R. W. Swanson. 1956. Soil Moisture Measurement by Neutron Moderation. *Soil Science* 82, 1 (1956), 29–42.
- [24] Marcelo Becker, Rafael Vidal Aroca, Daniel Varela Magalhães, and André Carmona Hernandes. 2016. Application of standard EPC/GEN2 UHF RFID tags as soil moisture sensors. In *Int Electron Conf Sens Applications*.
- [25] Jim Bilskie and Campbell Scientific. 2001. Soil water status: content and potential. *Campbell Scientific, Inc. App. Note: 2S-1* <http://s.campbellsci.com/documents/ca/technical-papers/soilh20c.pdf> (2 de Abril de 2014) (2001).
- [26] Lili Chen, Jie Xiong, Xiaojiang Chen, Sungsoon Ivan Lee, Kai Chen, Dianhe Han, Dingyi Fang, Zhanyong Tang, and Zheng Wang. 2019. WideSee: Towards Wide-Area Contactless Wireless Sensing. In *Proceedings of the 17th Conference on Embedded Networked Sensor Systems* (New York, New York) (*SenSys ’19*). Association for Computing Machinery, New York, NY, USA, 258–270.
- [27] Lien Chow, Zisheng Xing, Herb W. Rees, Fanrui Meng, John Monteith, and Lionel Stevens. 2009. Field Performance of Nine Soil Water Content Sensors on a Sandy Loam Soil in New Brunswick, Maritime Region, Canada. *Sensors (Basel, Switzerland)* 9 (2009), 9398 – 9413.
- [28] Thomas J. Dean, James P. Bell, and A. Baty. 1987. SOIL MOISTURE MEASUREMENT BY AN IMPROVED CAPACITANCE TECHNIQUE, PART I. SENSOR DESIGN AND PERFORMANCE. *Journal of Hydrology* 93 (1987), 67–78.
- [29] Pedro Dias, Doris Cadavid, Silvia Ortega, Alejandro Ruiz, Maria França, Flávio Moraes, Elnatan Ferreira, and Andreu Cabot. 2016. Autonomous soil moisture sensor based on nanostructured thermosensitive resistors powered by an integrated thermoelectric generator. *Sensors and Actuators A: Physical* 239 (01 2016).
- [30] Jian Ding and Ranveer Chandra. 2019. Towards Low Cost Soil Sensing Using Wi-Fi. In *The 25th Annual International Conference on Mobile Computing and Networking* (Los Cabos, Mexico) (*MobiCom ’19*). New York, NY, USA, Article 39.
- [31] Jagvir Dixit, R Gupta, V Behl, and Roshan Yadav. 2003. No-Tillage and Conventional Tillage System Evaluation for Production of Wheat - An Analysis. *Indian Journal of Agricultural Research* 37, 3 (2003), 199–203.
- [32] Ali Fares and Viktor Polyakov. 2006. Advances in Crop Water Management Using Capacitive Water Sensors. *Advances in Agronomy* 90 (12 2006), 43–77.
- [33] L. W. Galagedara, G. W. Parkin, J. D. Redman, Bertoldi P. Von, and A. L. Endres. 2000. Measuring Soil Water Content with Ground Penetrating Radar. In *Annual general meetings of ASA-CSSA-SSSA*.
- [34] W. Gardner and D. Kirkham. 1952. DETERMINATION OF SOIL MOISTURE BY NEUTRON SCATTERING. *Soil* 73, 5 (1952), 391–402.
- [35] Nitin A. Gawande, Debra R. Reinhardt, Philip A. Thomas, Philip T. McCreanor, and Timothy G. Townsend. 2003. Municipal solid waste in situ moisture content measurement using an electrical resistance sensor. *Waste Management* 23, 7 (2003), 667–674. Second Intercontinental Landfill Resarch Symposium.
- [36] David J Griffiths. 2013. *Introduction to electrodynamics* (4th. ed.). Pearson, Boston, MA.
- [37] Vinay Gupta, Sendil Kumar Devar, N. Hari Kumar, and Kala Praveen Bagadi. 2017. Modelling of IoT Traffic and Its Impact on LoRaWAN. In *GLOBECOM 2017 - 2017 IEEE Global Communications Conference*. 1–6.
- [38] Marcus Hardie. 2020. Review of Novel and Emerging Proximal Soil Moisture Sensors for Use in Agriculture. *Sensors* 20, 23 (2020), 6934.
- [39] Jetmir Haxhibeqiri, Abdulkadir Karaagac, Floris Van den Abeele, Wout Joseph, Ingrid Moerman, and Jeroen Hoebeke. 2017. LoRa indoor coverage and performance in an industrial environment: Case study. In *2017 22nd IEEE International Conference on Emerging Technologies and Factory Automation (ETFA)*. 1–8.

- [40] M. A. Hilhorst, K Van Breugel, Djmh Pluimgraaff, and W. S. Kroesea. 1995. Dielectric Sensors used in Environmental and Construction Engineering. *Mrs Proceedings* 411 (1995), 401.
- [41] Daniel Hillel. 2013. *Introduction to soil physics*. Academic press.
- [42] S. S. Hubbard, Jr J. E. Peterson, E. L. Majer, P. T. Zawislanski, K. H. Williams, J. Roberts, and Frank Wobber. 1997. Estimation of permeable pathways and water content using tomographic radar data. *The Leading Edge* 16, 11 (1997), 1623–1630.
- [43] Thomas J. Jackson. 1993. III. Measuring surface soil moisture using passive microwave remote sensing. *Hydrological Processes* (1993).
- [44] Tala Kanso, Marie-Christine Gromaire, David Ramier, Philippe Dubois, and Ghassan Chebbo. 2020. An Investigation of the Accuracy of EC5 and 5TE Capacitance Sensors for Soil Moisture Monitoring in Urban Soils—Laboratory and Field Calibration. *Sensors (Basel, Switzerland)* 20, 22 (11 2020), 6510.
- [45] Kai-Hsiang Ke, Qi-Wen Liang, Guan-Jie Zeng, Jun-Han Lin, and Huang-Chen Lee. 2017. Demo Abstract: A LoRa Wireless Mesh Networking Module for Campus-Scale Monitoring. In *2017 16th ACM/IEEE International Conference on Information Processing in Sensor Networks (IPSN)*. 259–260.
- [46] T.J. Kellener, Richard Soppe, David Robinson, M. Schaap, J.E. Ayars, and Todd Skaggs. 2004. Calibration of Capacitance Probe Sensors using Electric Circuit Theory. *Soil Sci. Soc. Am. J.* 68 (03 2004).
- [47] A. Klotzsche, F. Jonard, M. C. Looms, J. Van Der Kruk, and J. A. Huisman. 2018. Measuring Soil Water Content with Ground Penetrating Radar: A Decade of Progress. *Vadose Zone Journal* 17, 1 (2018).
- [48] Mihai T. Lazarescu. 2013. Design of a WSN Platform for Long-Term Environmental Monitoring for IoT Applications. *IEEE Journal on Emerging and Selected Topics in Circuits and Systems* 3, 1 (2013), 45–54.
- [49] Jian Li, T. Hong, R. Feng, X. Yue, and Yuju Luo. 2011. High-frequency capacitive soil water content sensor based on detecting of true root mean square. *Nongye Gongcheng Xuebao/Transactions of the Chinese Society of Agricultural Engineering* 27 (08 2011), 216–221.
- [50] Yuxiang Lin, Wei Dong, Yi Gao, and Tao Gu. 2020. SateLoc: A Virtual Fingerprinting Approach to Outdoor LoRa Localization using Satellite Images. In *2020 19th ACM/IEEE International Conference on Information Processing in Sensor Networks (IPSN)*.
- [51] Jun Liu, Jiayao Gao, Sanjay Jha, and Wen Hu. 2021. Seirios: Leveraging Multiple Channels for LoRaWAN Indoor and Outdoor Localization (*MobiCom '21*). Association for Computing Machinery, New York, NY, USA, 656–669.
- [52] Sujuan Liu, Chuyu Xia, and Zhenzhen Zhao. 2016. A low-power real-time air quality monitoring system using LPWAN based on LoRa. In *2016 13th IEEE International Conference on Solid-State and Integrated Circuit Technology (ICSICT)*. 379–381.
- [53] Ian R. McCann, Dennis C. Kincaid, and D. Wang. 1992. Operational Characteristics of the Watermark Model 200 Soil Water Potential Sensor for Irrigation Management. *Applied Engineering in Agriculture* 8 (1992), 603–609.
- [54] Rajalakshmi Nandakumar, Vikram Iyer, and Shyamnath Gollakota. 2018. 3D Localization for Sub-Centimeter Sized Devices. *ACM* (2018).
- [55] DA Robinson, CS Campbell, JW Hopmans, Brian K Hornbuckle, Scott B Jones, R Knight, F Ogden, J Selker, and O Wendroth. 2008. Soil moisture measurement for ecological and hydrological watershed-scale observatories: A review. *Vadose Zone Journal* 7, 1 (2008), 358–389.
- [56] Hafiz Husnain Raza Sherazi, Muhammad Ali Imran, Gennaro Boggia, and Luigi Alfredo Grieco. 2018. Energy Harvesting in LoRaWAN: A Cost Analysis for the Industry 4.0. *IEEE Communications Letters* 22, 11 (2018), 2358–2361.
- [57] R. L. Smith-Rose. 1933. The Electrical Properties of Soil for Alternating Currents at Radio Frequencies. *Proceedings of the Royal Society of London. Series A, Containing Papers of a Mathematical and Physical Character* 140, 841 (1933), 359–377.
- [58] Philipp Sommer, Yannick Maret, and Dacfey Dzung. 2018. Low-Power Wide-Area Networks for Industrial Sensing Applications. In *2018 IEEE International Conference on Industrial Internet (ICI)*. 23–32.
- [59] Marios Sophocleous, Andreas Karkotis, and Julius Georgiou. 2021. A Versatile, Stand-Alone, In-Field Sensor Node for Implementation in Precision Agriculture. *IEEE Journal on Emerging and Selected Topics in Circuits and Systems* 11, 3 (2021), 449–457.
- [60] Sun and G. D. Young. 2001. A COST EFFECTIVE SOIL MOISTURE INSTRUMENT BASED ON TIME-DOMAIN TRANSMISSION MEASUREMENT.
- [61] P Sérgio, G. Nathan, and B. John. 2018. Two Solutions of Soil Moisture Sensing with RFID for Landslide Monitoring. *Sensors* 18, 2 (2018), 452.
- [62] A M Thomas. 1966. In situ measurement of moisture in soil and similar substances by 'fringe' capacitance. 43, 1 (jan 1966), 21–27.
- [63] G. C. Topp, J. L. Davis, and A. P. Annan. 1980. Electromagnetic determination of soil water content: Measurements in coaxial transmission lines. *Water Resources Research* 16, 3 (1980), 574–582.
- [64] Marc Van Iersel, R.M. Seymour, Matthew Chappell, F. Watson, and S. Dove. 2009. Soil moisture sensor-based irrigation reduces water use and nutrient leaching in a commercial nursery. *Proc. Southern Nursery Assn. Res. Conf.* 54 (01 2009), 17–21.
- [65] C. D. van Loon. 1981. The effect of water stress on potato growth, development, and yield. *American Potato Journal* 58, 1 (1981), 51–69.
- [66] Van Anh Vu, Dong Cong Trinh, Tuan Christian TRUVANT, and Thanh Dang Bui. 2018. Design of automatic irrigation system for greenhouse based on LoRa technology. In *2018 International Conference on Advanced Technologies for Communications (ATC)*. 72–77.
- [67] Ju Wang, Liqiong Chang, Shourya Aggarwal, Omid Abari, and Srinivasan Keshav. 2020. Soil Moisture Sensing with Commodity RFID Systems (*MobiSys '20*). New York, NY, USA, 273–285.

- [68] J. R. Wang and B. J. Choudhury. 1981. Remote sensing of soil moisture content, over bare field at 1.4 GHz frequency. *Journal of Geophysical Research: Oceans* 86, C6 (1981).
- [69] Wesseling and J. 1983. Soil Water Assessment by the Neutron Method. *Agricultural Water Management* 6, 1 (1983), 79.
- [70] Xianjin Xia, Ningning Hou, Yuanqing Zheng, and Tao Gu. 2021. PCube: Scaling LoRa Concurrent Transmissions with Reception Diversities. In *Proceedings of the 27th Annual International Conference on Mobile Computing and Networking* (New Orleans, Louisiana) (*MobiCom '21*). Association for Computing Machinery, New York, NY, USA, 670–683.
- [71] Binbin Xie and Jie Xiong. 2020. Combating Interference for Long Range LoRa Sensing. In *Proceedings of the 18th Conference on Embedded Networked Sensor Systems* (Virtual Event, Japan) (*SensSys '20*). Association for Computing Machinery, New York, NY, USA, 69–81.
- [72] Binbin Xie, Yuqing Yin, and Jie Xiong. 2021. Pushing the Limits of Long Range Wireless Sensing with LoRa. 5, 3, Article 134 (Sept. 2021), 21 pages.
- [73] Adrian Zarnescu, Razvan Ungurelu, Mihai Secere, Gaudentiu Varzaru, and Bogdan Mihailescu. 2020. Implementing a large LoRa network for an agricultural application. In *2020 7th International Conference on Energy Efficiency and Agricultural Engineering (EE AE)*. 1–5.
- [74] Fusang Zhang, Zhaoxin Chang, Kai Niu, Jie Xiong, Beihong Jin, Qin Lv, and Daqing Zhang. 2020. Exploring LoRa for Long-Range Through-Wall Sensing. 4, 2, Article 68 (2020), 27 pages.
- [75] Fusang Zhang, Zhaoxin Chang, Jie Xiong, Rong Zheng, Junqi Ma, Kai Niu, Beihong Jin, and Daqing Zhang. 2021. Unlocking the Beamforming Potential of LoRa for Long-Range Multi-Target Respiration Sensing. 5, 2, Article 85 (June 2021), 25 pages.
- [76] Liang Zhao, Wenyan Wu, and Shengming Li. 2019. Design and Implementation of an IoT-Based Indoor Air Quality Detector With Multiple Communication Interfaces. *IEEE Internet of Things Journal* 6, 6 (2019), 9621–9632.